Supplementary Information

Synthesis, Characterization, Photophysics, and Anion Binding Properties of Platinum(II) Acetylide Complexes with Urea Group

Zhi-Hui Zhang, Jiewei Liu, Li-Qi Wan, Fang-Ru Jiang, Chi-Keung Lam, Bao-Hui Ye, Zhengping Qiao, and Hsiu-Yi Chao*

MOE Key Laboratory of Bioinorganic and Synthetic Chemistry, School of Chemistry and Chemical Engineering, Sun Yat-Sen University, Guangzhou 510275, P. R. China

E-mail: zhaoxy@mail.sysu.edu.cn; Fax: +86-20-84112245; Tel: +86-20-84110062.

Table S1. Crystallographic data of **3a**, **3a**·DMF·THF, **3b**·CH_3CN, and **3c**·CH_3CN

	3a	**3a**·DMF·THF	**3b**·CH_3CN	**3c**·CH_3CN
Formula	$C_{43}H_{46}F_3N_5O_4PtS$	$C_{50}H_{46}F_3N_6O_6PtS$	$C_{45}H_{45}ClF_3N_6O_4PtS$	$C_{46}H_{48}F_6N_6O_4PtS$
Formula weight	981.01	1111.10	1053.49	1090.05
Temperature/K	150.0	298.0	150.0	173.0
Crystal system	triclinic	monoclinic	monoclinic	monoclinic
Space group	P-1	$P2_1/n$	$P2_1/n$	$P2_1/n$
a/Å	9.3035(4)	12.1155(3)	14.3112(8)	14.39500(10)
b/Å	12.0230(5)	29.9363(5)	14.7141(7)	14.86570(10)
c/Å	20.6666(5)	15.1278(4)	20.9907(8)	21.4413(2)
α/°	88.269(3)	90.00	90.00	90.00
β/°	87.144(2)	112.253(3)	95.457(1)	95.4310(10)
γ/°	79.980(3)	90.00	90.00	90.00
V/$Å^3$	2273.04(14)	5078.1(2)	4400.1(4)	4567.66(6)
Z	2	4	4	4
ρ_{calc} (mg/mm^3)	1.4332	1.4532	1.5902	1.585
Refns collected	21510	27099	30853	23402
Indep reflns	9422	7758	9644	7249
R_{int}	0.0505	0.0659	0.0607	0.0357
GOF	1.193	1.146	1.026	1.026
R,[a] R_w[b] [≥2σ (I)]	0.0576, 0.1619	0.0559, 0.1447	0.0474, 0.1412	0.0329, 0.0816

[a] $R = \Sigma(|F_o| - |F_c|) / \Sigma|F_o|$. [b] $R_w = [\Sigma w(|F_o| - |F_c|)^2 / \Sigma w|F_o|^2]^{1/2}$

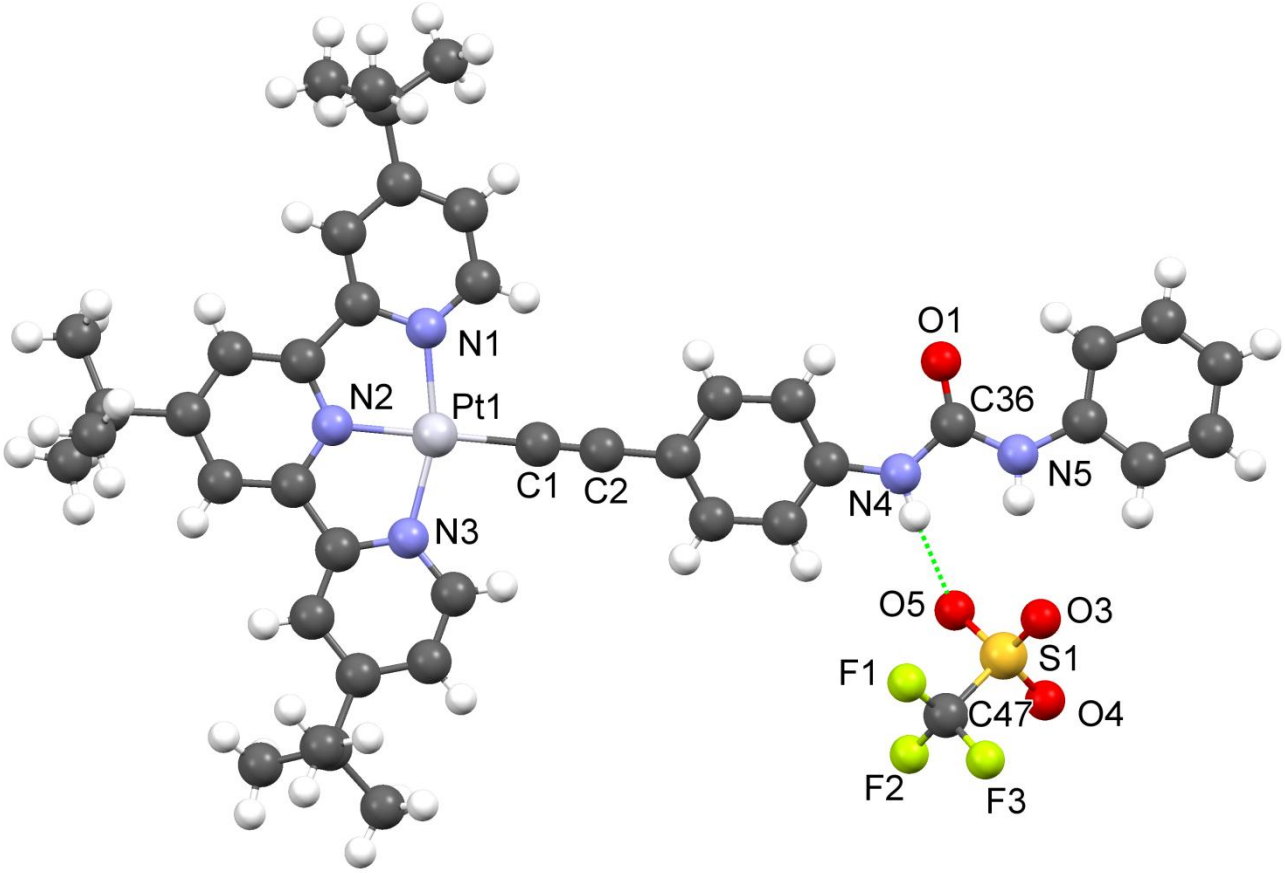

Figure S1. Perspective view of **3a**·DMF·THF. Solvent molecules have been omitted for clarity.

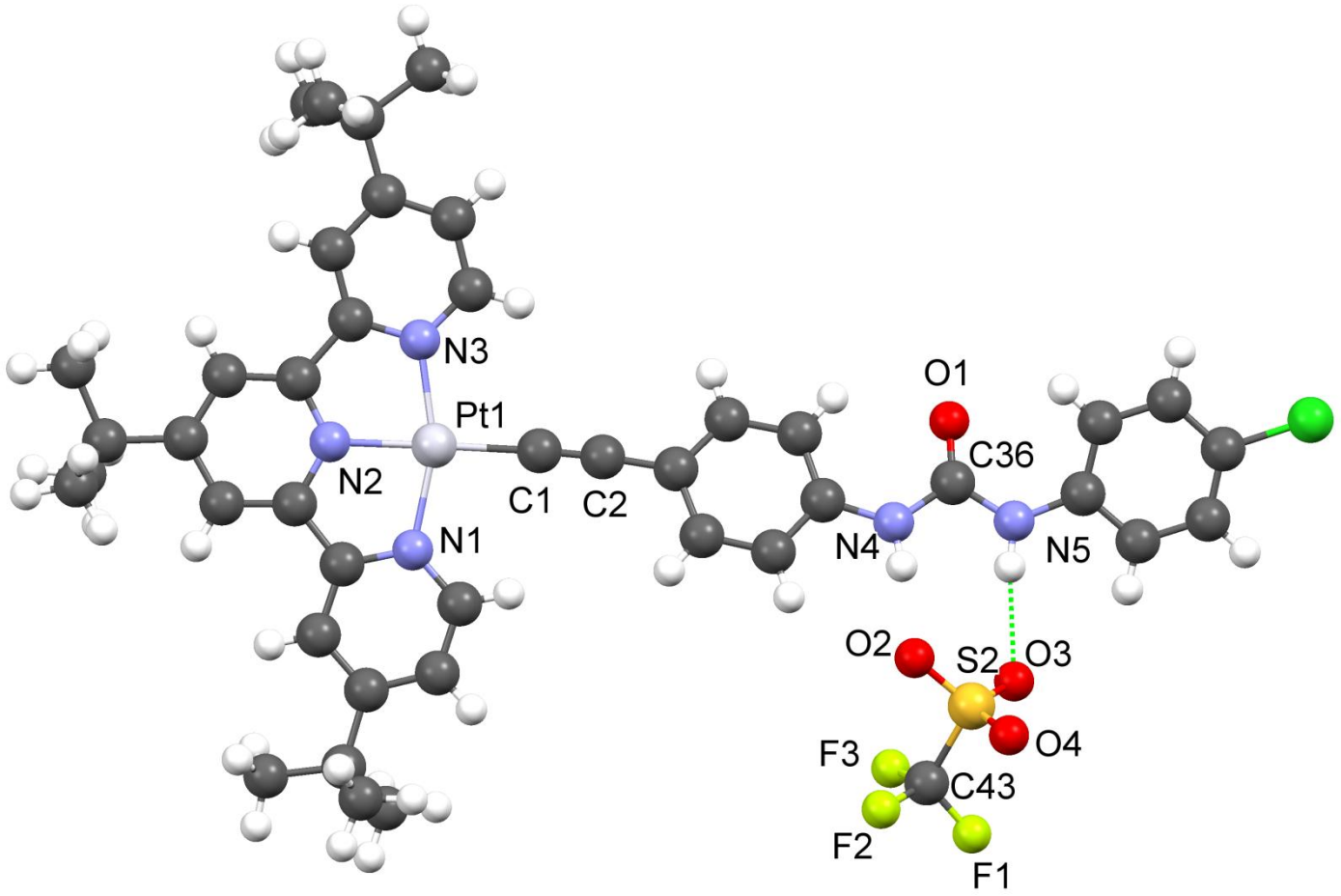

Figure S2. Perspective view of **3b**·CH_3CN. Solvent molecules have been omitted for clarity.

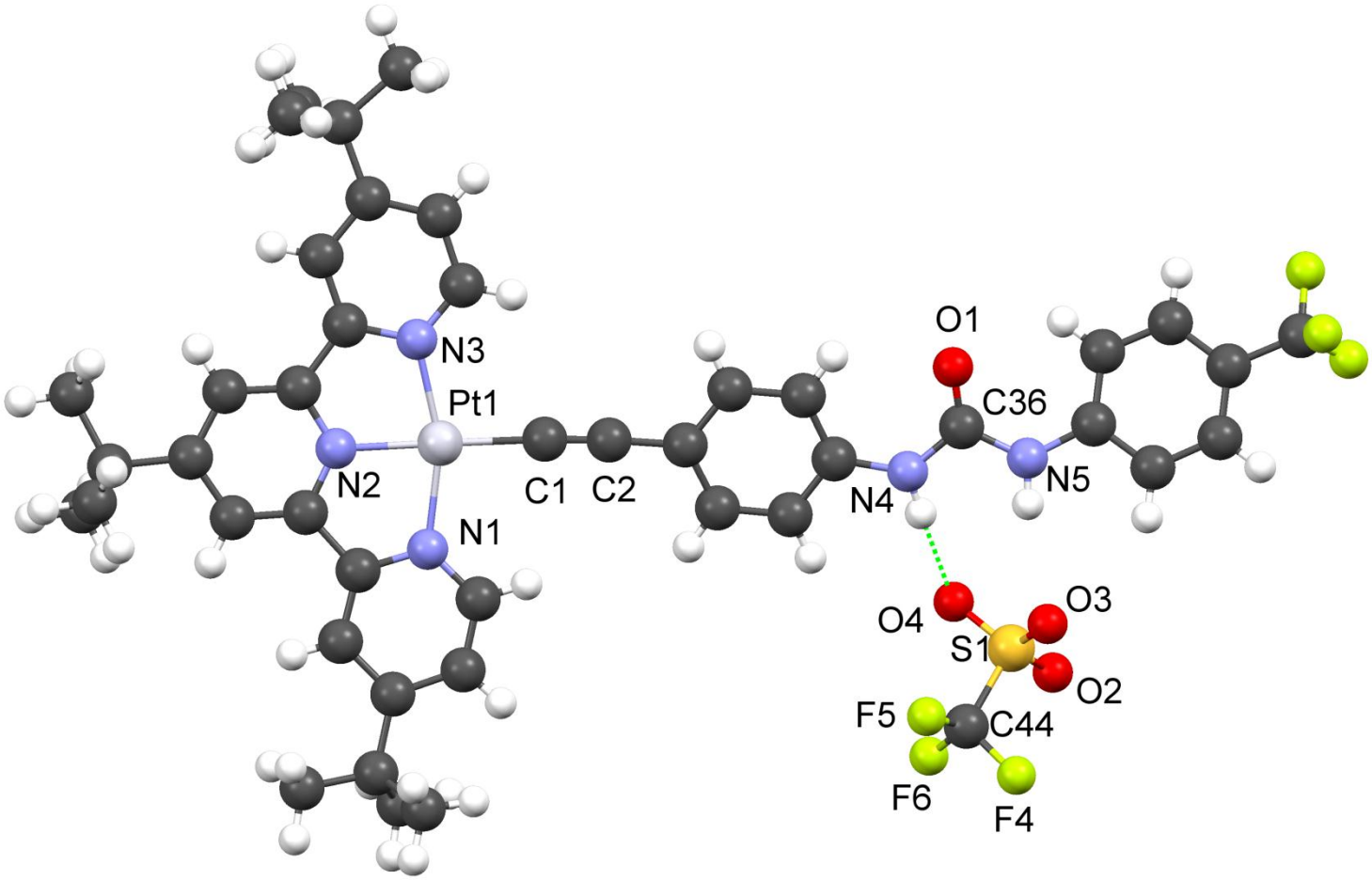

Figure S3. Perspective view of **3c**·CH_3CN. Solvent molecules have been omitted for clarity.

Table S2. Hydrogen bond parameters (N–H···O) of **3a**, **3a**·DMF·THF, **3b**·CH_3CN and **3c**·CH_3CN (Å and °)

complex	D–H···A	d(D–H)	d(H···A)	d(D···A)	∠(DHA)
3a	N(4)–H(7)···O(3)[a]	0.880	2.192	3.062	169.84
3a·DMF·THF	N(4)–H(30)···O(5)[b]	0.860	2.111	2.953	166.30
3b·CH_3CN	N(4)–H(37)···O(2)[b]	0.880	2.022	2.887	166.81
3c·CH_3CN	N(4)–H(1A)···O(4)[b]	0.880	2.065	2.927	169.6 1

[a]Symmetry transformations used to generate equivalent atoms: –x, –y, –z.
[b]Symmetry transformations used to generate equivalent atoms: 1/2–x, 1/2+y, 1/2–z.

Table S3. Photophysical data of ligands **1a–1d** at 298 K

compound	medium	λ_{abs}/nm (ε/$dm^3 \cdot mol^{-1} \cdot cm^{-1}$)	λ_{em}/nm
1a	CH_3CN	274 (50300)	318, 398
1b	CH_3CN	275 (53860)	316, 406
1c	CH_3CN	276 (67440)	314, 413
1d	CH_3CN	263 (29160), 333 (28000)	Non-emissive

Table S4. The low-energy absorption maximum (nm) of **3a** and **3b** in various solvents at 298 K and the corresponding dielectric constant of the solvents

	CH_2Cl_2	THF	$CH_3C(O)CH_3$	DMSO	CH_3CN	CH_3OH
3a	498	492	476	472	464	458
3b	502	493	-	469	460	453
dielectric constant	8.9	7.6	20.7	46.7	37.5	24.5

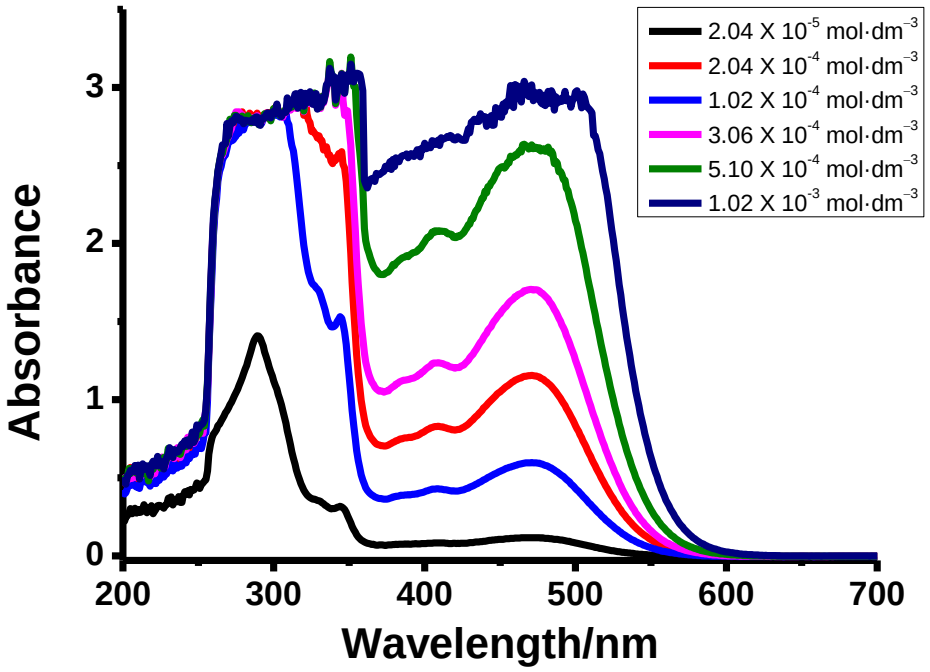

Figure S4. The electronic absorption spectral changes of **3a** as the concentration increase from 1×10^{-5} to 1×10^{-3} mol· dm^{-3} at 298 K.

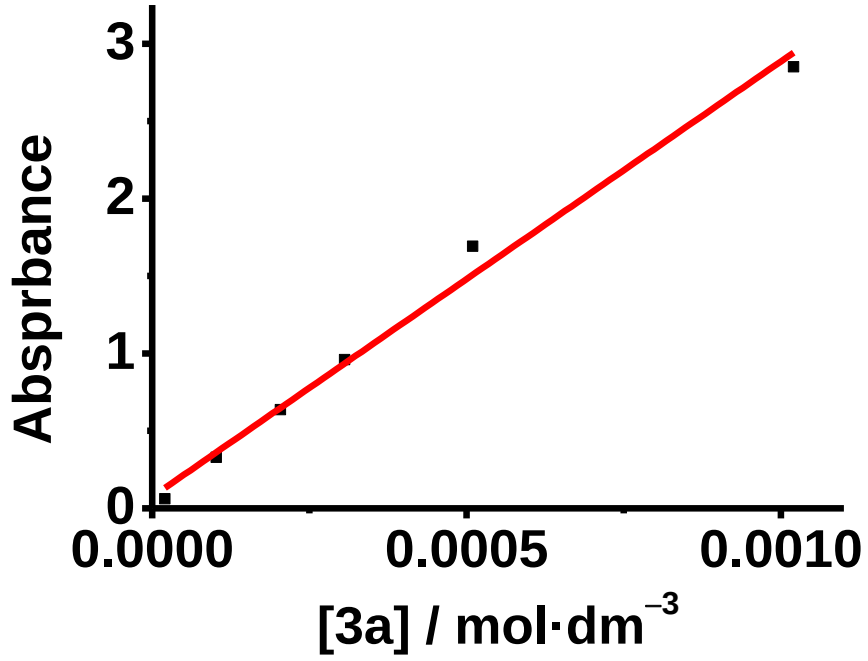

Figure S5. Plot of the absorbance at 510 nm as a function of concentration.

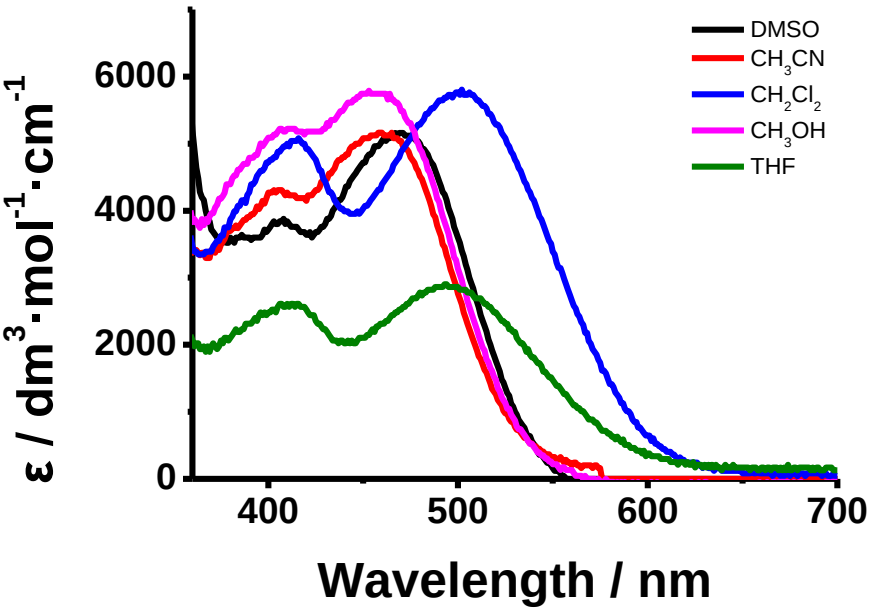

Figure S6. Electronic absorption spectrum of **3b** in various solutions at 298 K at 360-700 nm

(a)

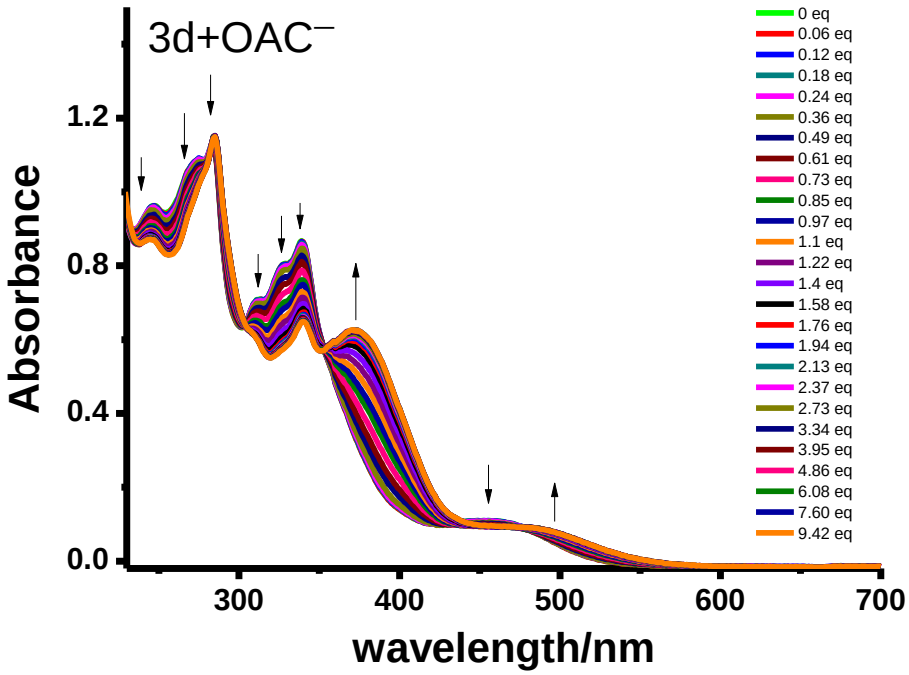

(b)

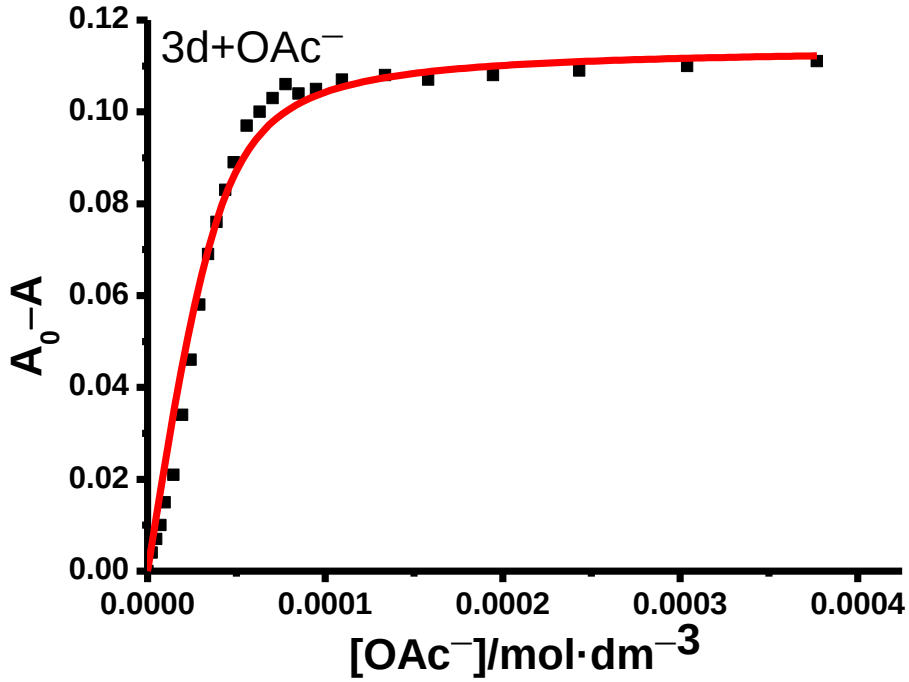

Figure S7. (a) UV–vis spectral changes of **3d** (4×10^{-5} mol·dm^{-3}) in CH_3CN upon addition of OAc^-. (b) A plot of the absorbance change at 254 nm as a function of the concentration of OAc^- and its theoretical fit for the 1:1 binding of complex **3d** with OAc^-.

(a)

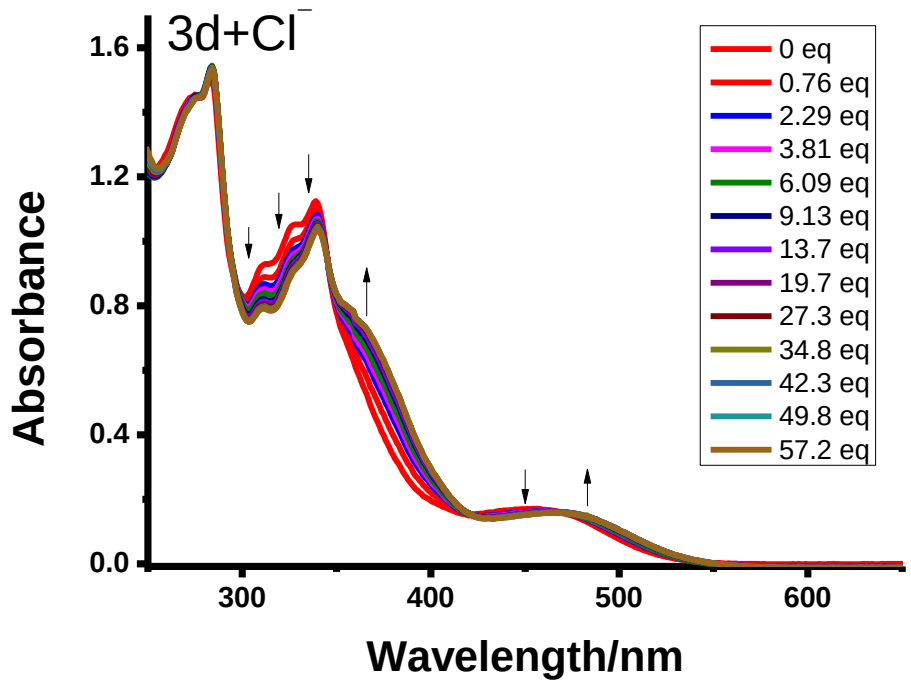

(b)

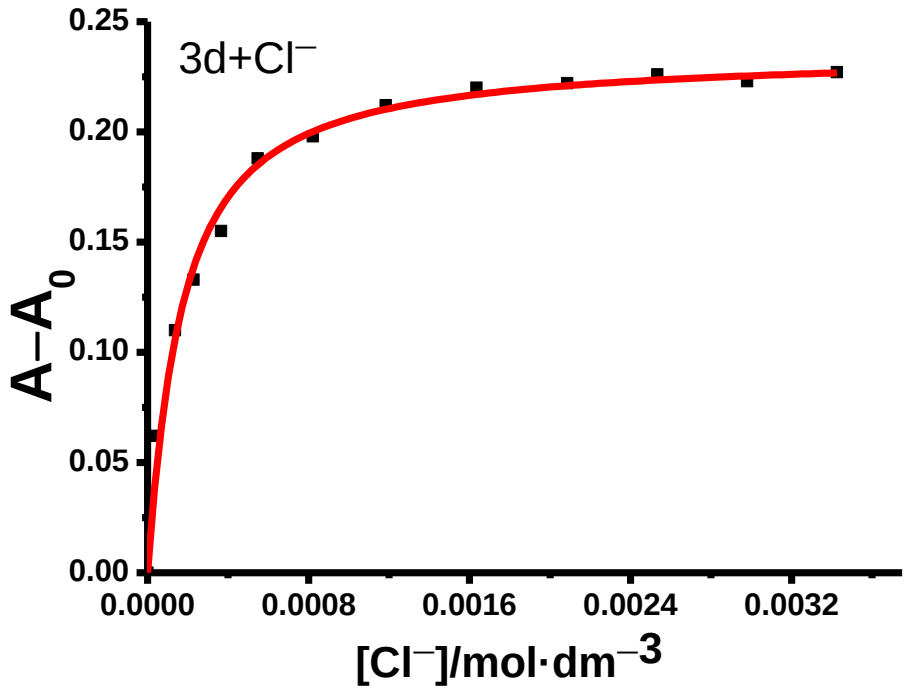

Figure S8. (a) UV–vis spectral changes of **3d** (4×10^{-5} mol·dm^{-3}) in CH_3CN upon addition of Cl^-. (b) A plot of the absorbance change at 370 nm as a function of the concentration of Cl^- and its theoretical fit for the 1:1 binding of complex **3d** with Cl^-.

(a)

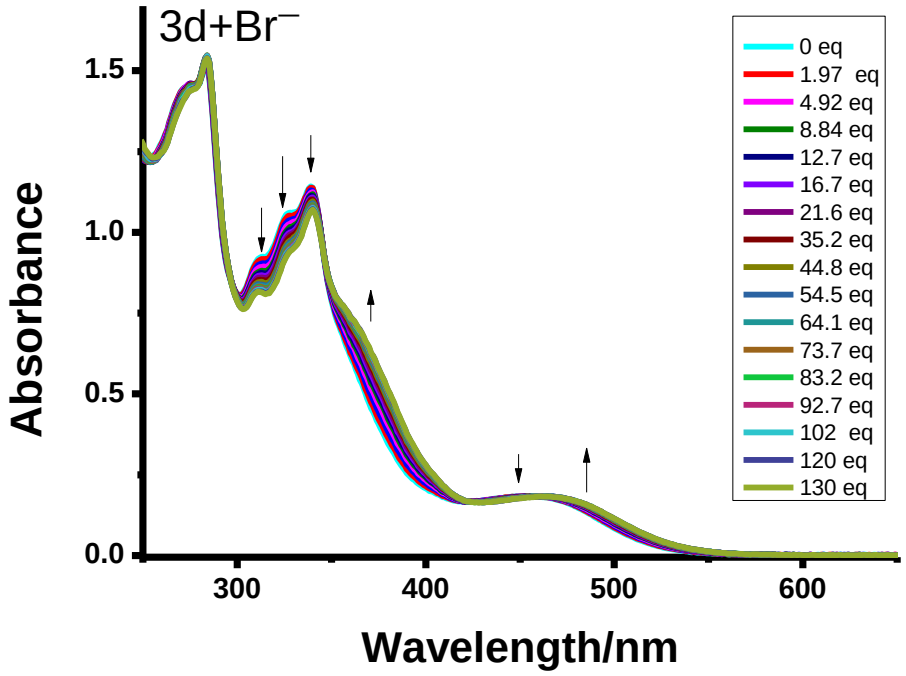

(b)

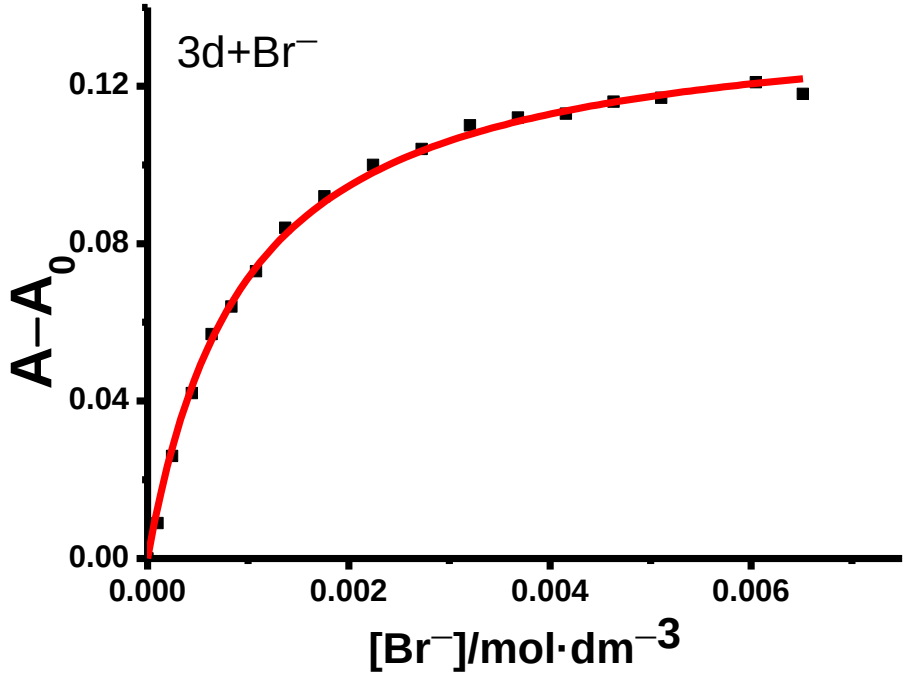

Figure S9. (a) UV–vis spectral changes of **3d** (5×10^{-5} mol·dm^{-3}) in CH_3CN upon addition of Br^-. (b) A plot of the absorbance change at 360 nm as a function of the concentration of Br^- and its theoretical fit for the 1:1 binding of complex **3d** with Br^-.

(a)

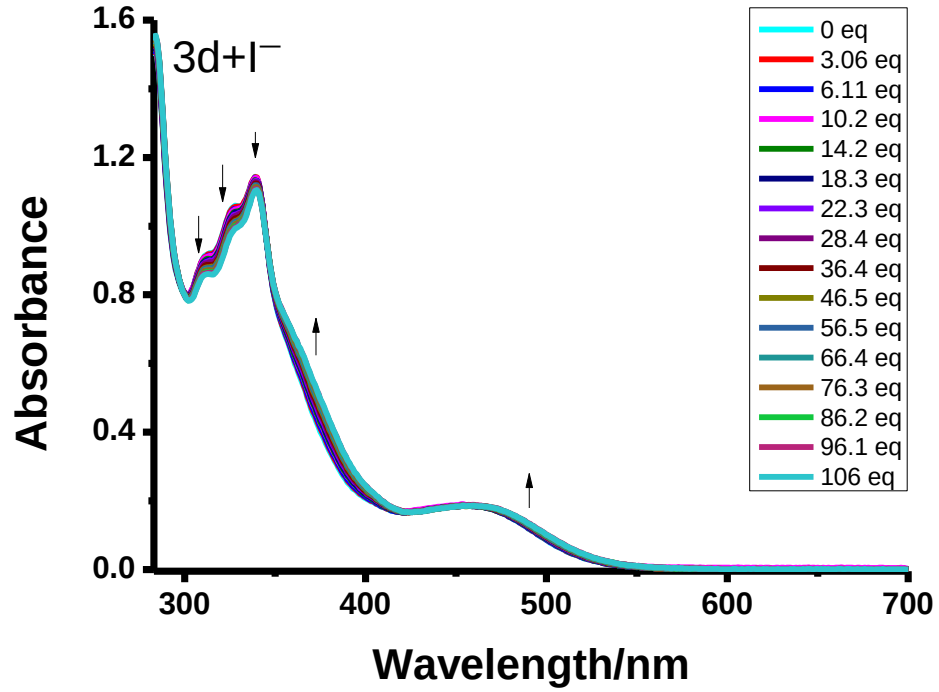

(b)

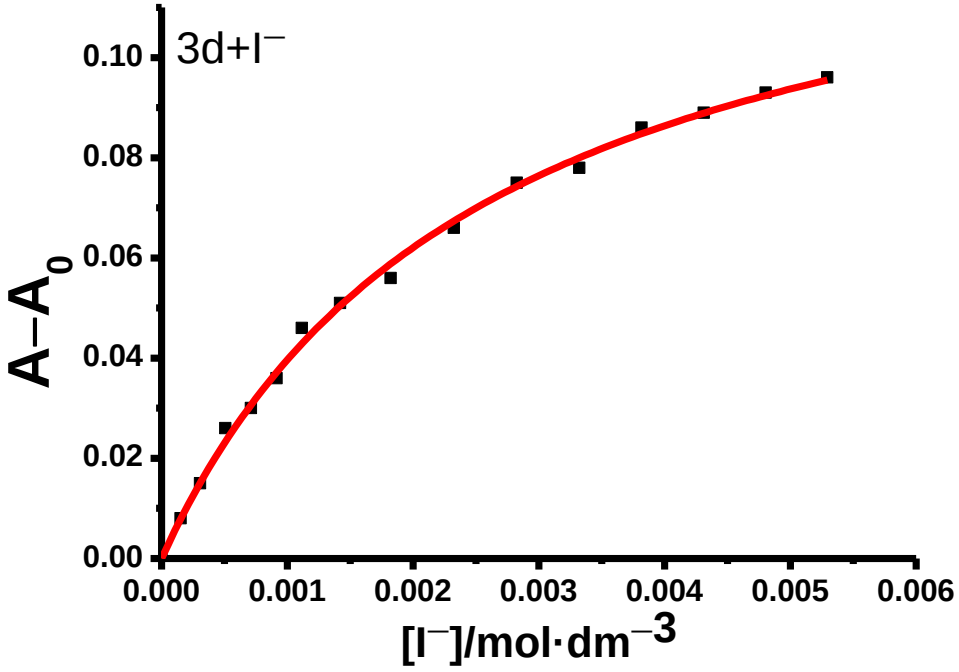

Figure S10. (a) UV–vis spectral changes of **3d** (5×10^{-5} mol·dm^{-3}) in CH_3CN upon addition of I^-. (b) A plot of the absorbance change at 370 nm as a function of the concentration of I^- and its theoretical fit for the 1:1 binding of complex **3d** with I^-.

(a)

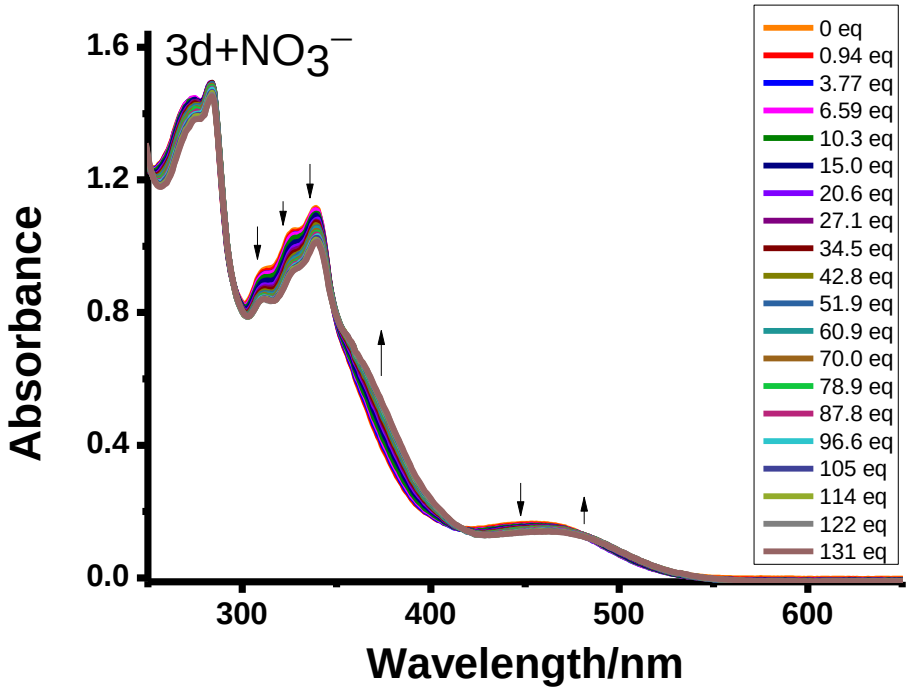

(b)

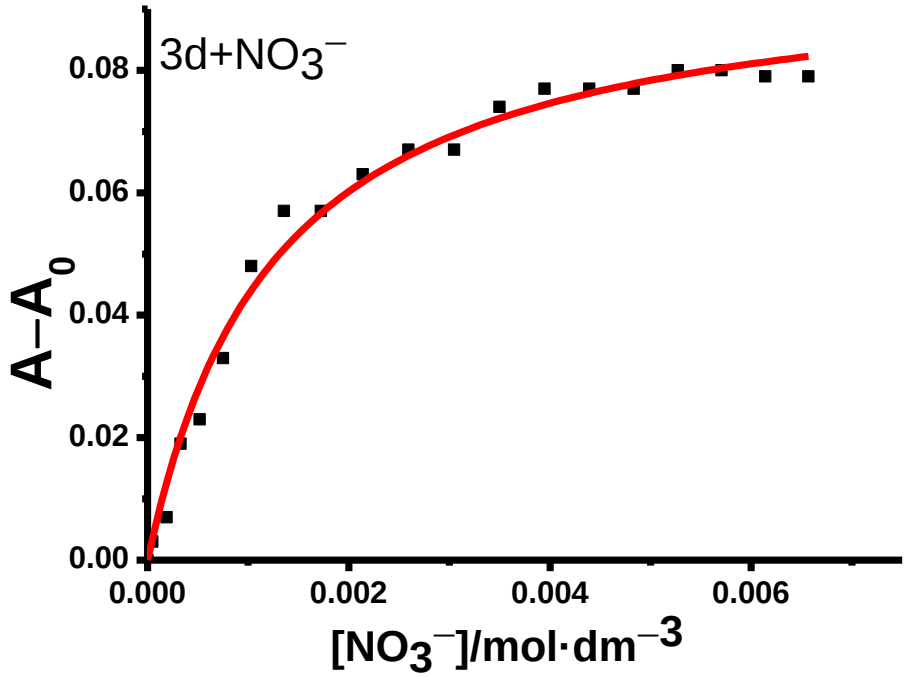

Figure S11. (a) UV–vis spectral changes of **3d** (5×10^{-5} mol·dm^{-3}) in CH_3CN upon addition of NO_3^-. (b) A plot of the absorbance change at 360 nm as a function of the concentration of NO_3^- and its theoretical fit for the 1:1 binding of complex **3d** with NO_3^-.

(a)

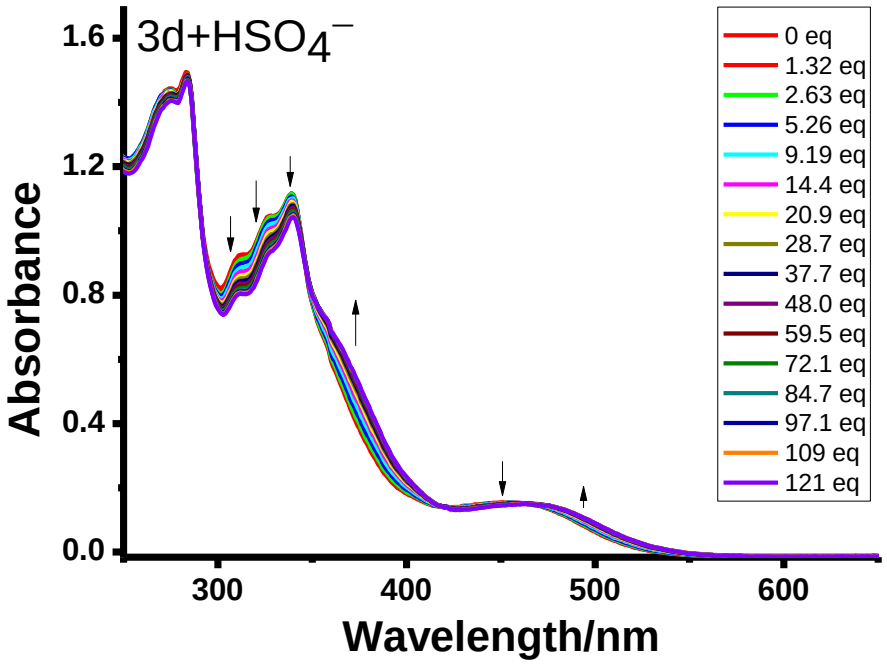

(b)

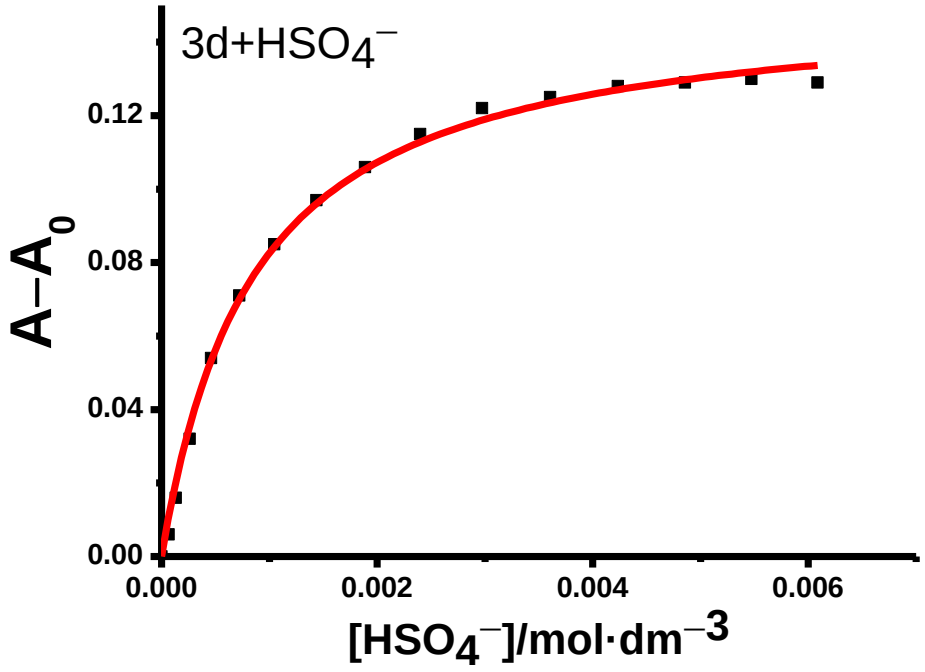

Figure S12. (a) UV–vis spectral changes of **3d** (5×10^{-5} mol·dm^{-3}) in CH_3CN upon addition of HSO_4^-. (b) A plot of the absorbance change at 368 nm as a function of the concentration of HSO_4^- and its theoretical fit for the 1:1 binding of complex **3d** with HSO_4^-.

(a)

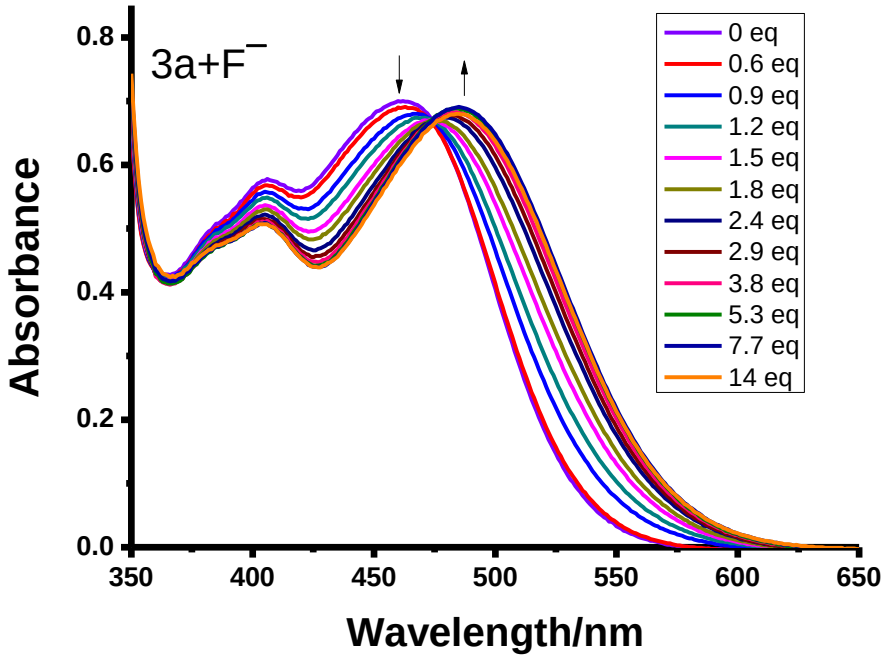

(b)

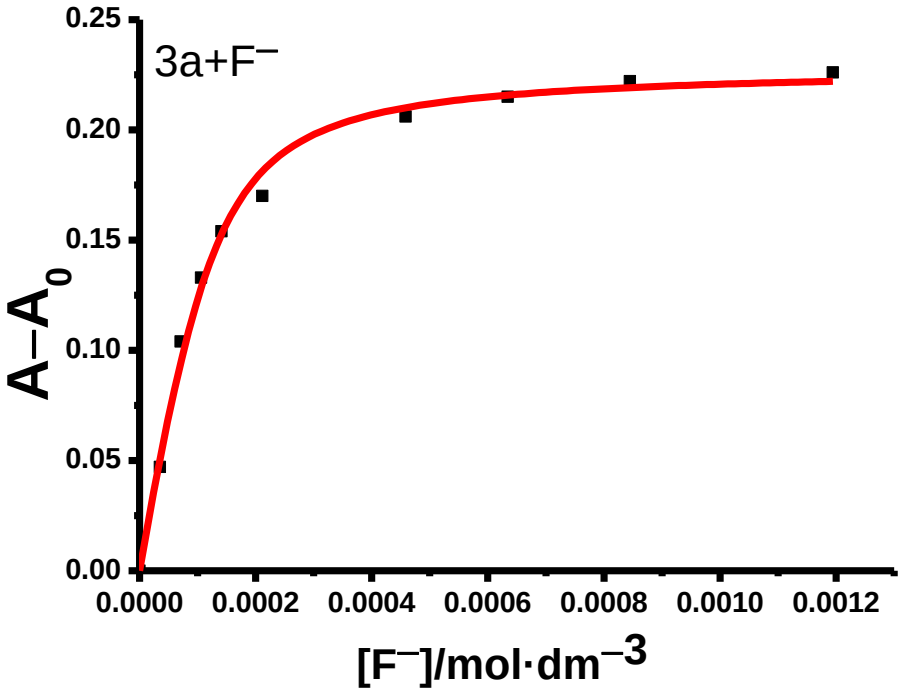

Figure S13. (a) UV–vis spectral changes of **3a** (1.2×10^{-4} mol·dm^{-3}) in CH_3CN upon addition of F^-. (b) A plot of the absorbance change at 510 nm as a function of the concentration of F^- and its theoretical fit for the 1:1 binding of complex **3a** with F^-.

(a)

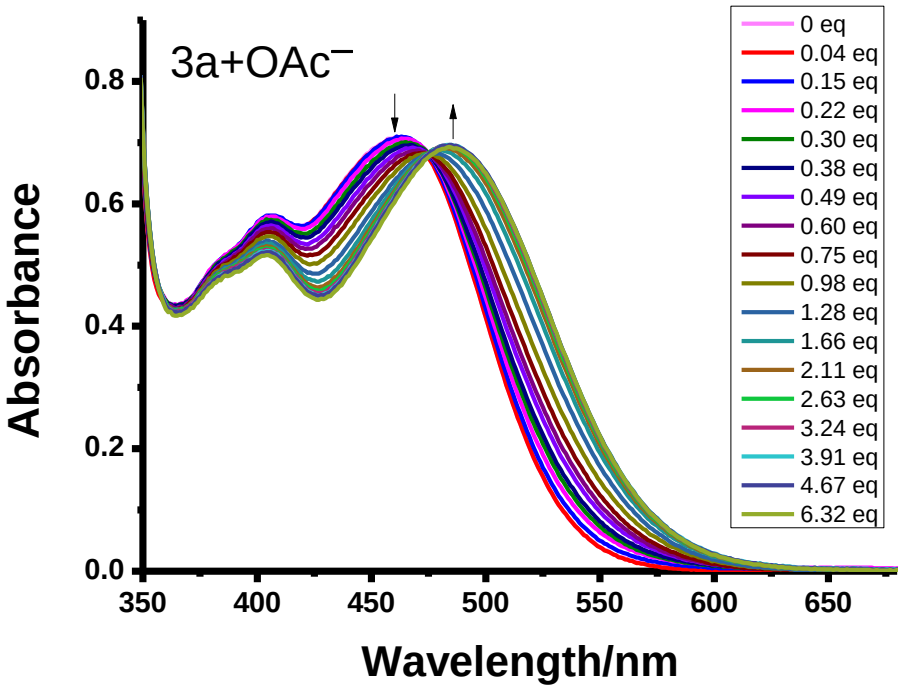

(b)

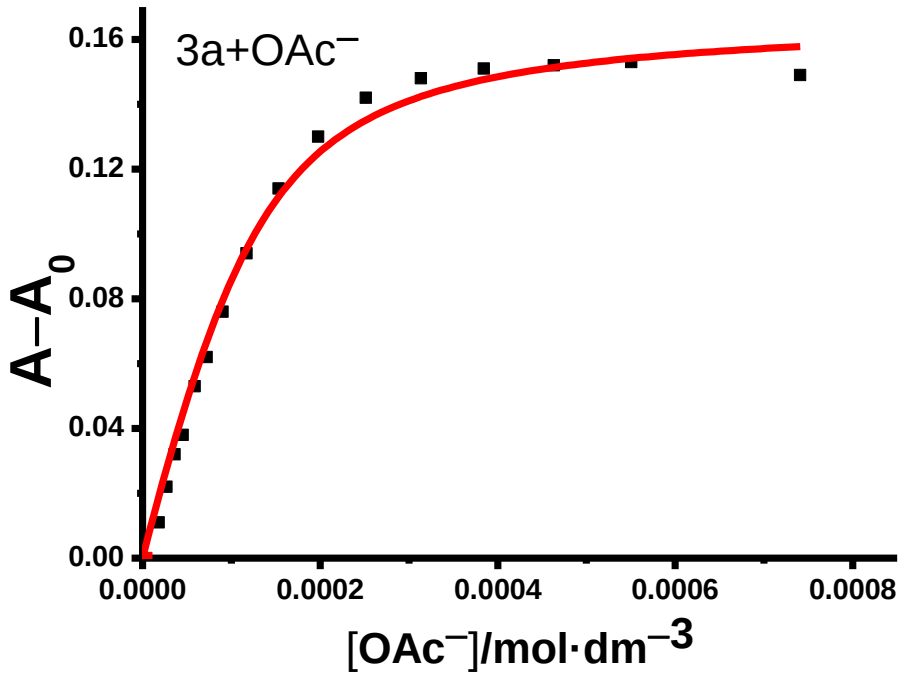

Figure S14. (a) UV–vis spectral changes of **3a** (1.2×10^{-4} mol·dm^{-3}) in CH_3CN upon addition of OAc^-. (b) A plot of the absorbance change at 490 nm as a function of the concentration of OAc^- and its theoretical fit for the 1:1 binding of complex **3a** with OAc^-.

(a)

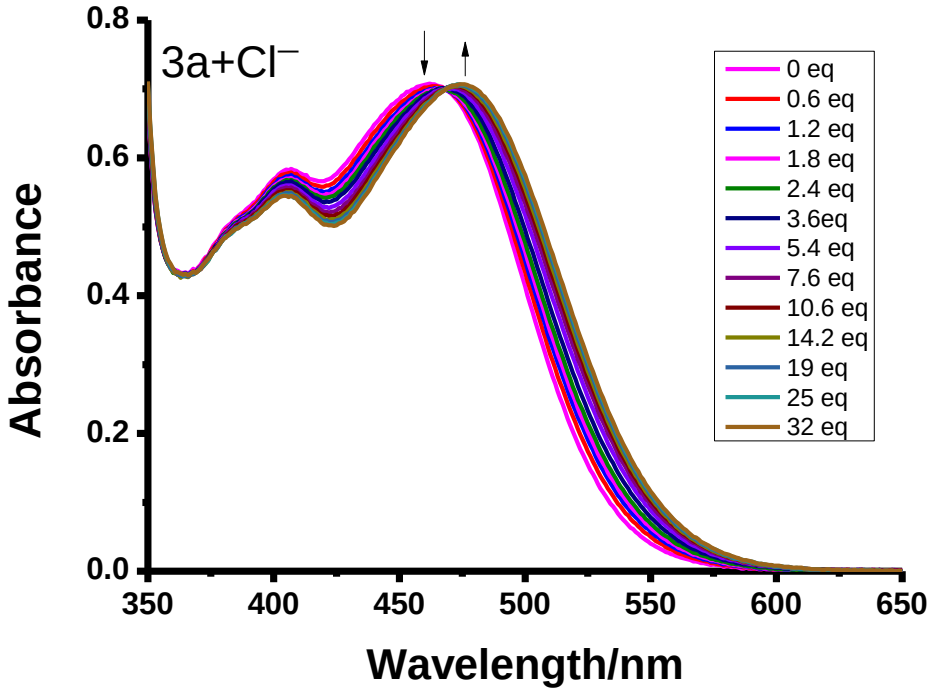

(b)

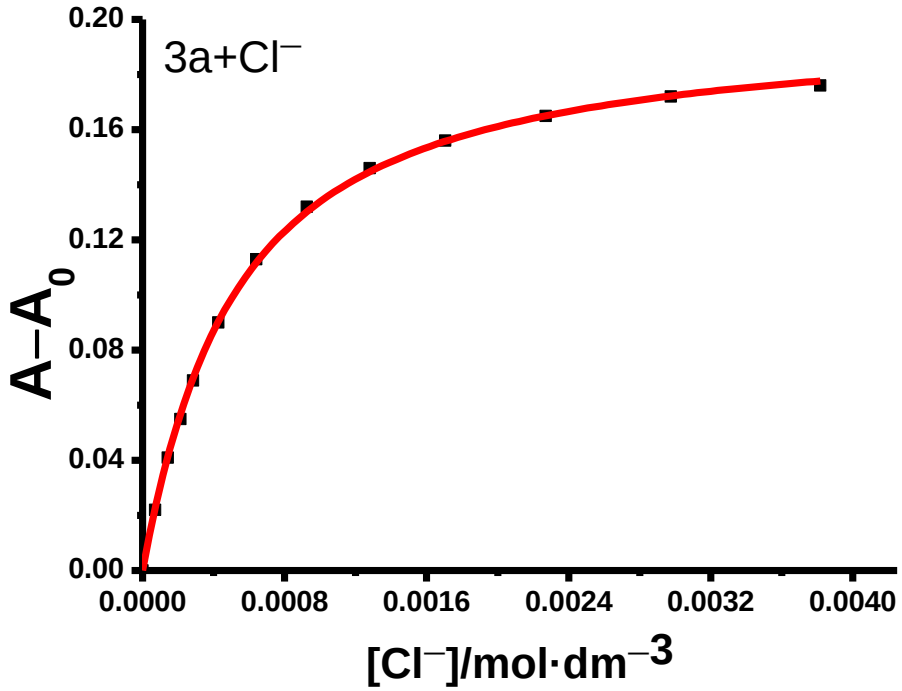

Figure S15. (a) UV–vis spectral changes of **3a** (1.2×10^{-4} mol·dm^{-3}) in CH_3CN upon addition of Cl^-. (b) A plot of the absorbance change at 510 nm as a function of the concentration of Cl^- and its theoretical fit for the 1:1 binding of complex **3a** with Cl^-.

(a)

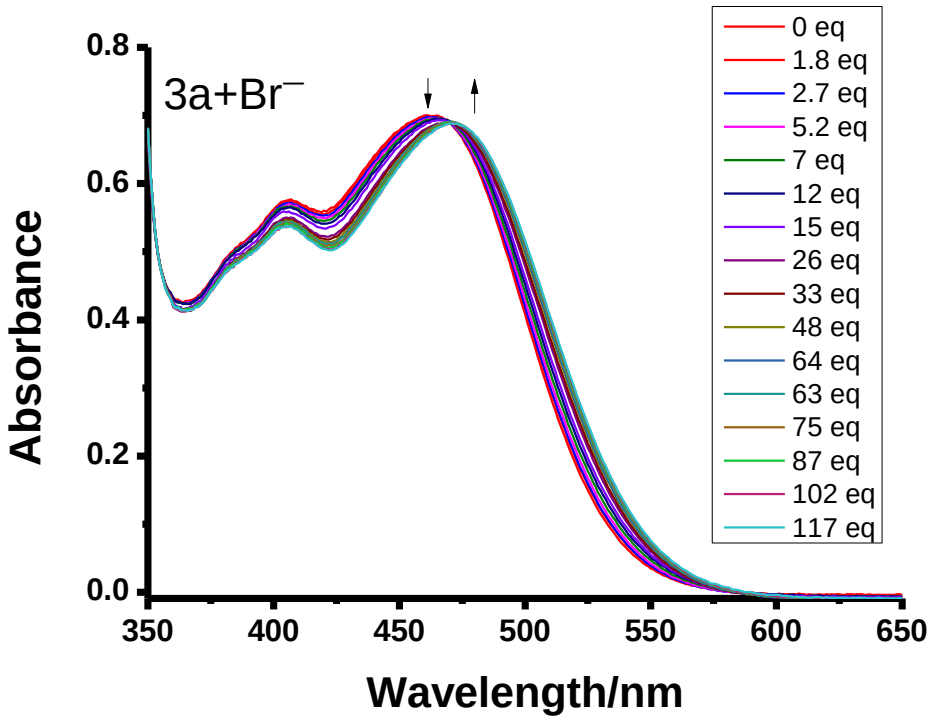

(b)

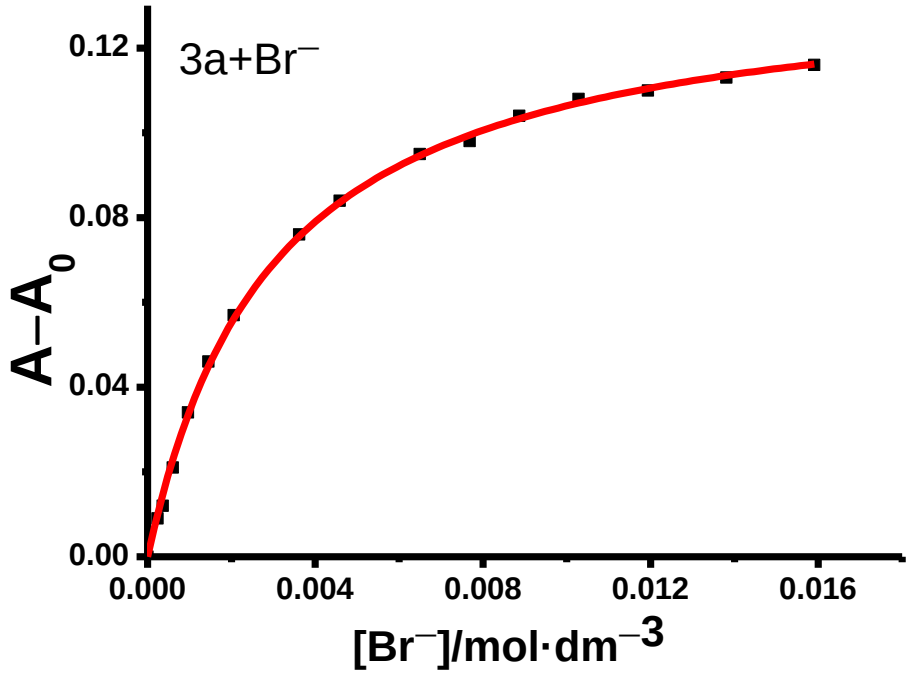

Figure S16. (a) UV–vis spectral changes of **3a** (1.2×10^{-4} mol·dm^{-3}) in CH_3CN upon addition of Br^-. (b) A plot of the absorbance change at 510 nm as a function of the concentration of Br^- and its theoretical fit for the 1:1 binding of complex **3a** with Br^-.

(a)

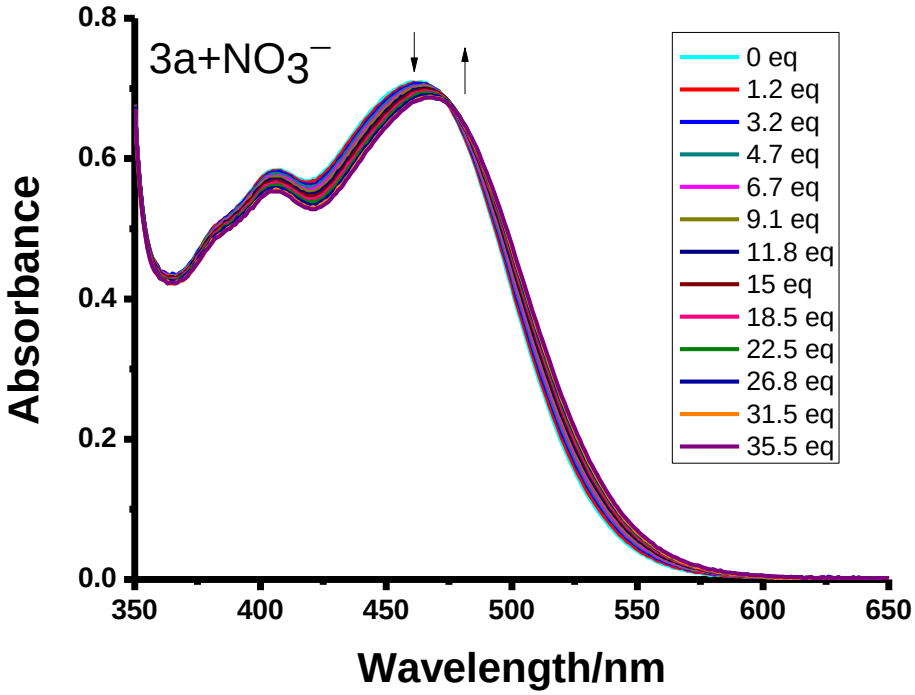

(b)

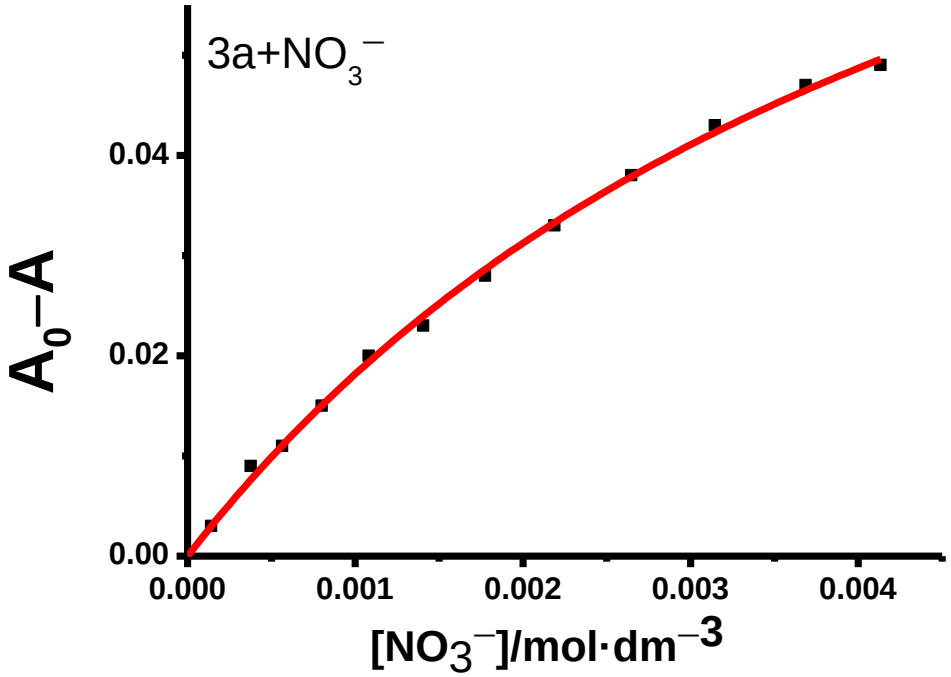

Figure S17. (a) UV–vis spectral changes of **3a** (1.2×10^{-4} mol·dm^{-3}) in CH_3CN upon addition of NO_3^-. (b) A plot of the absorbance change at 430 nm as a function of the concentration of NO_3^- and its theoretical fit for the 1:1 binding of complex **3a** with NO_3^-.

(a)

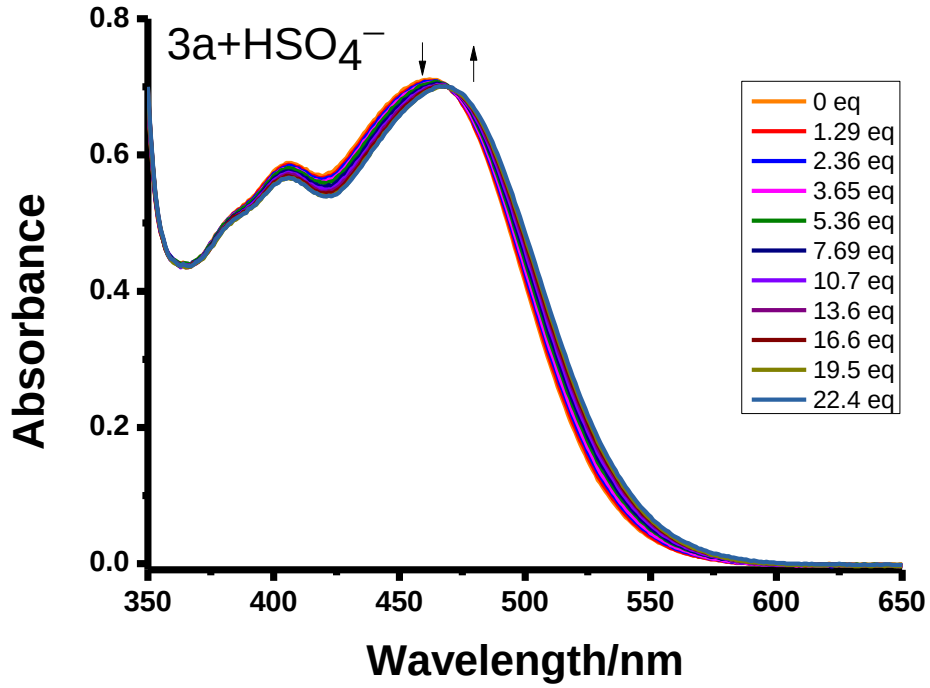

(b)

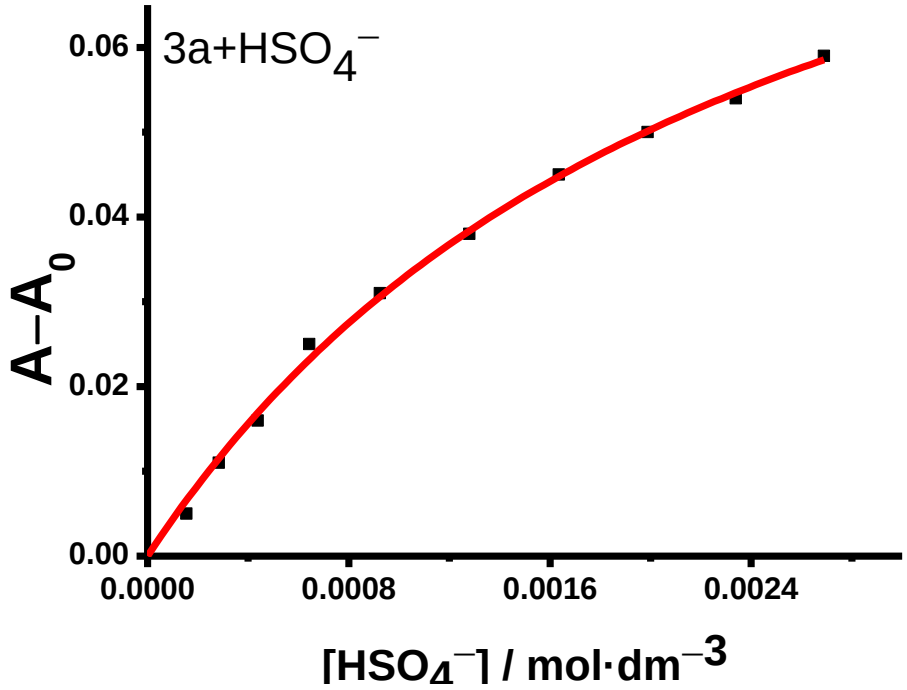

Figure S18. (a) UV–vis spectral changes of **3a** (1.2×10^{-4} mol·dm^{-3}) in CH_3CN upon addition of HSO_4^-. (b) A plot of the absorbance change at 530 nm as a function of the concentration of HSO_4^- and its theoretical fit for the 1:1 binding of complex **3a** with HSO_4^-.

(a)

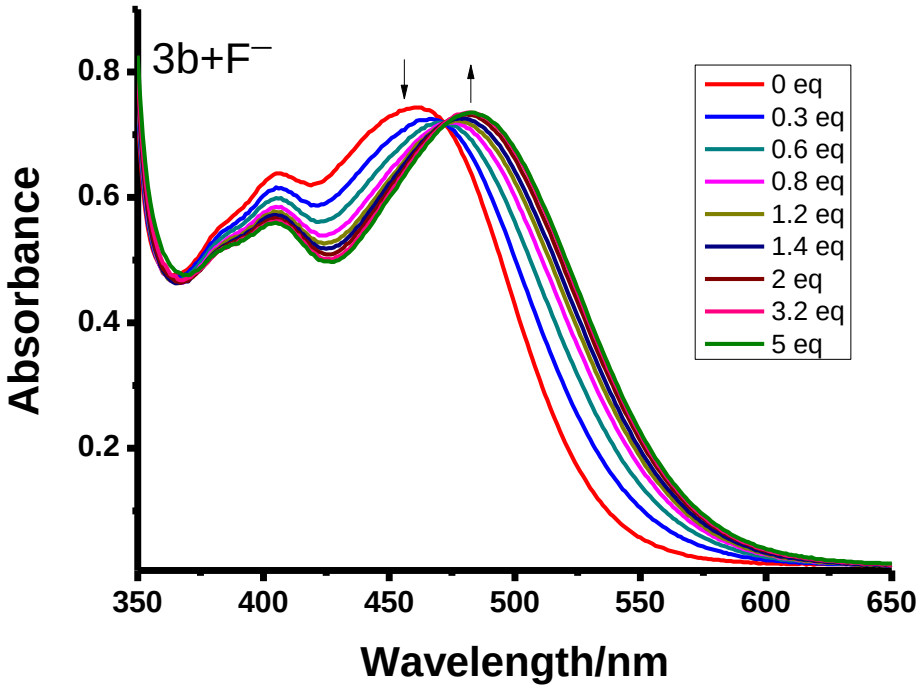

(b)

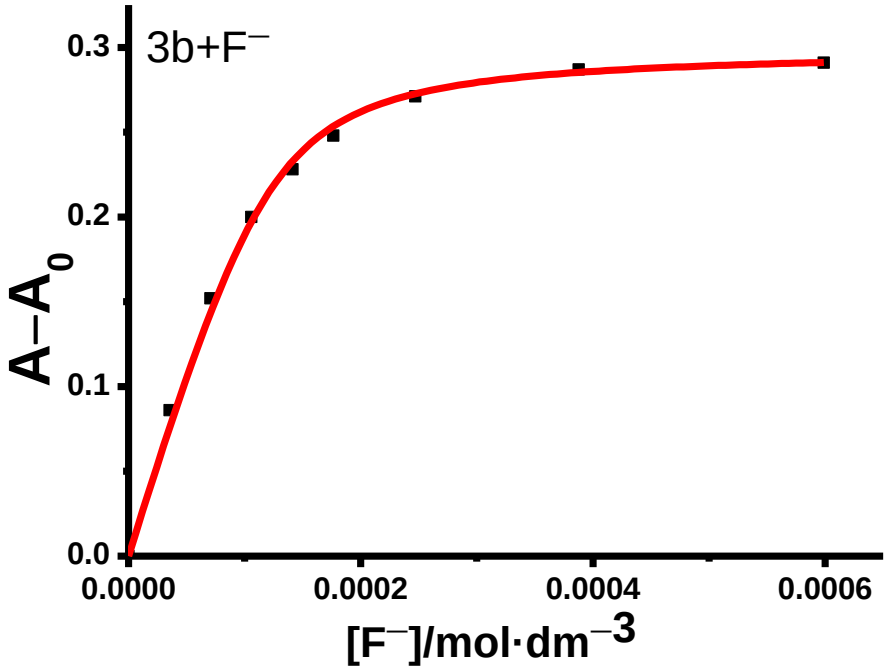

Figure S19. (a) UV–vis spectral changes of **3b** (1.2×10^{-4} mol·dm^{-3}) in CH_3CN upon addition of F^-. (b) A plot of the absorbance change at 510 nm as a function of the concentration of F^- and its theoretical fit for the 1:1 binding of complex **3b** with F^-.

(a)

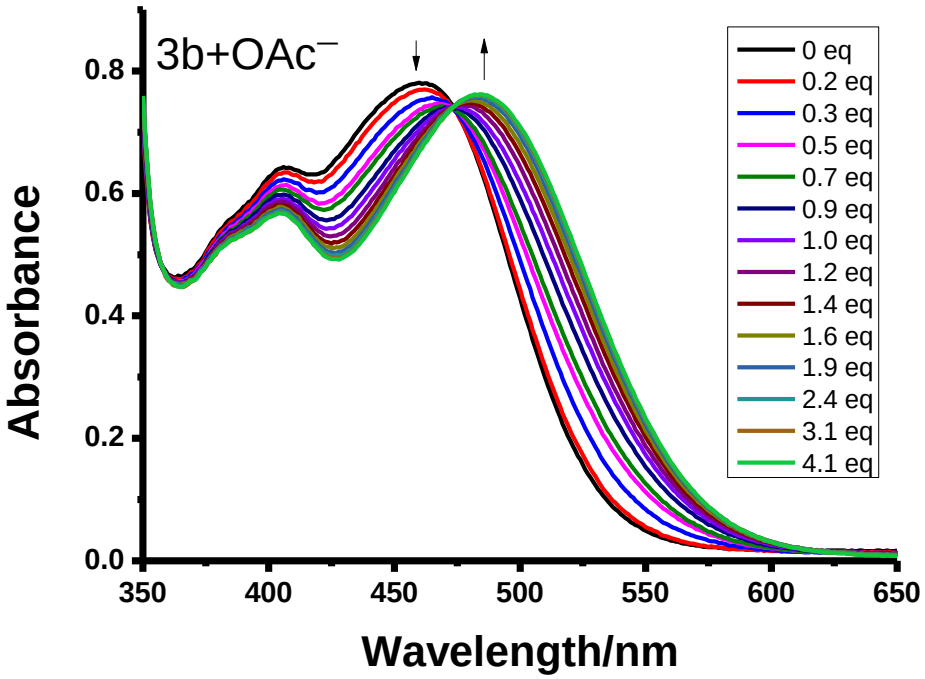

(b)

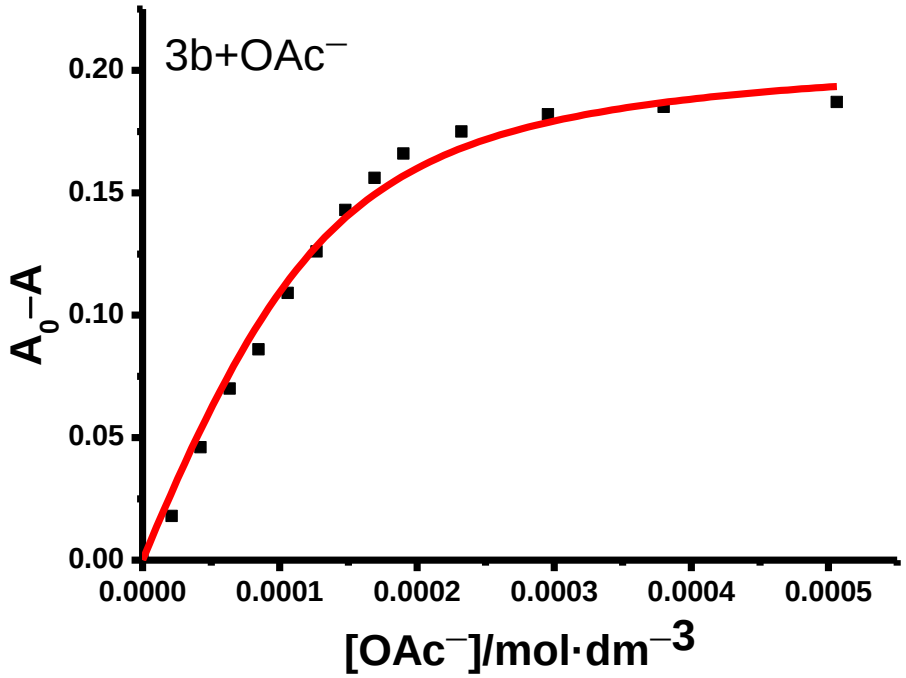

Figure S20. (a) UV–vis spectral changes of **3b** (1.2×10^{-4} mol·dm^{-3}) in CH_3CN upon addition of OAc^-. (b) A plot of the absorbance change at 440 nm as a function of the concentration of OAc^- and its theoretical fit for the 1:1 binding of complex **3b** with OAc^-.

(a)

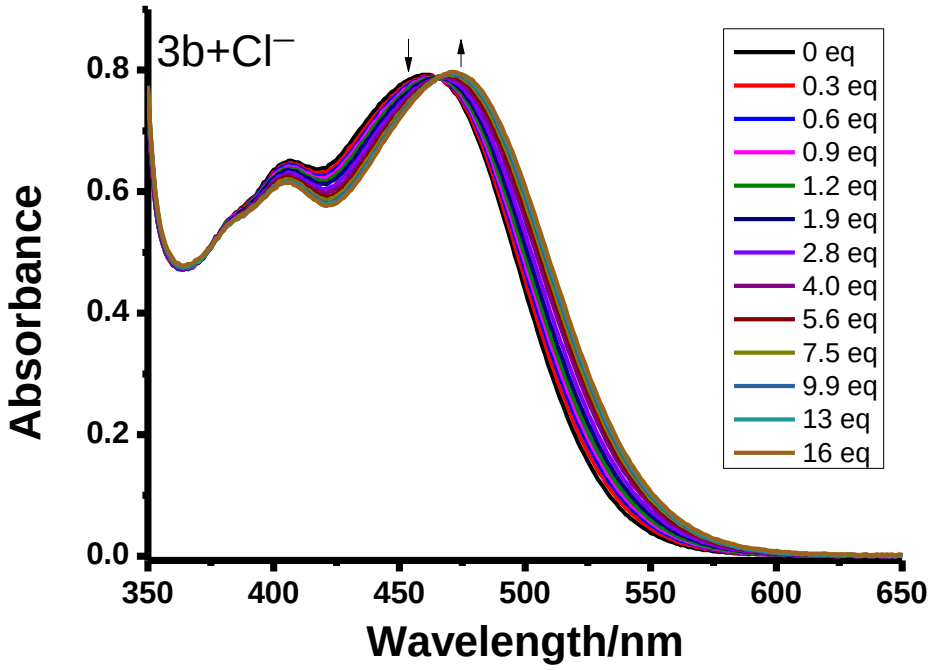

(b)

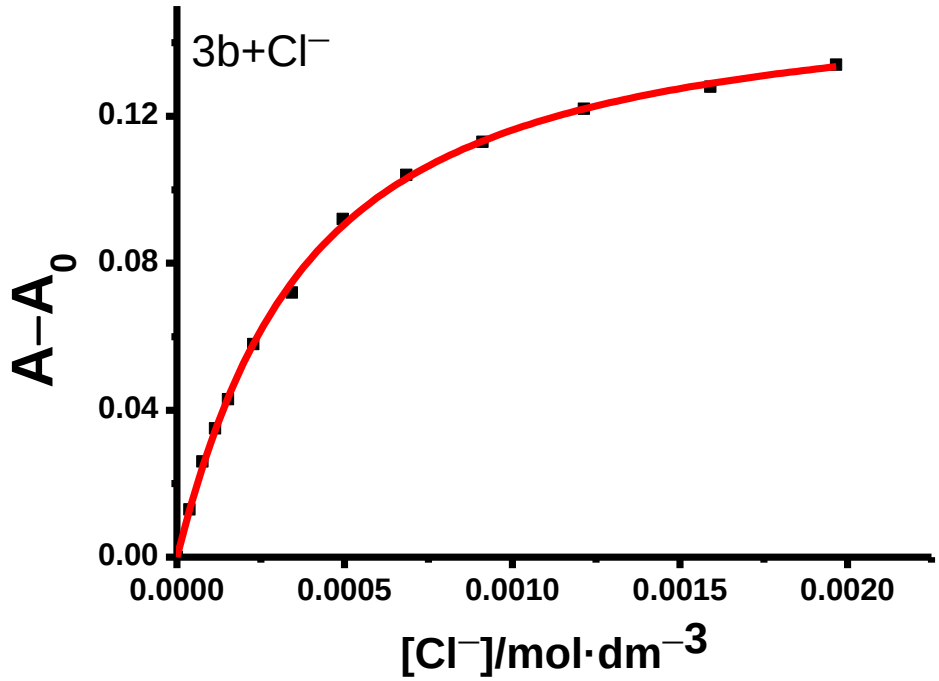

Figure S21. (a) UV–vis spectral changes of **3b** (1.2×10^{-4} mol·dm^{-3}) in CH_3CN upon addition of Cl^-. (b) A plot of the absorbance change at 490 nm as a function of the concentration of Cl^- and its theoretical fit for the 1:1 binding of complex **3b** with Cl^-.

(a)

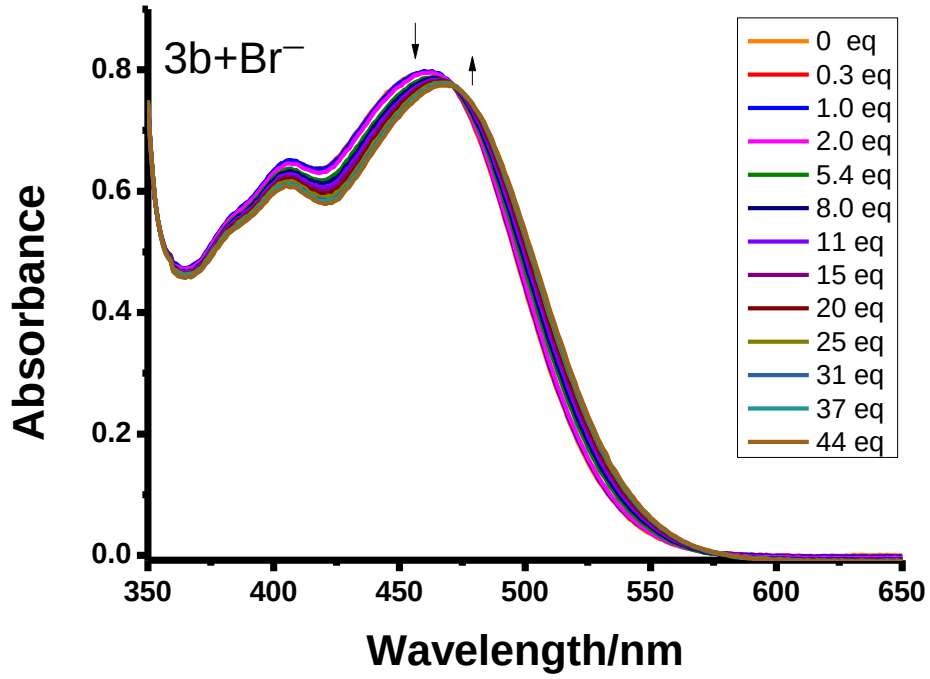

(b)

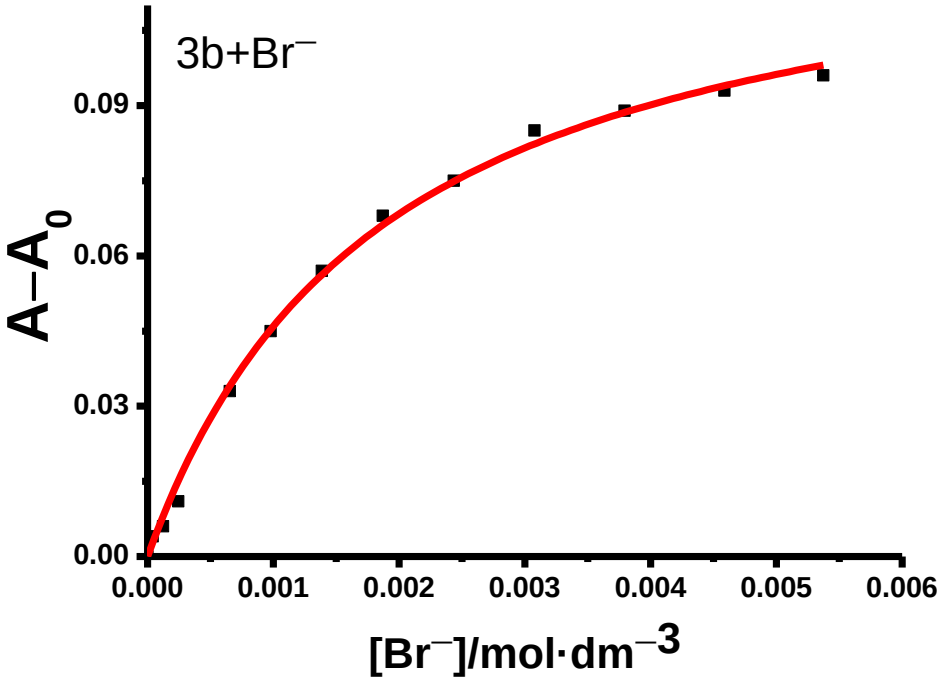

Figure S22. (a) UV–vis spectral changes of **3b** (1.2×10^{-4} mol·dm^{-3}) in CH_3CN upon addition of Br^-. (b) A plot of the absorbance change at 500 nm as a function of the concentration of Br^- and its theoretical fit for the 1:1 binding of complex **3b** with Br^-.

(a)

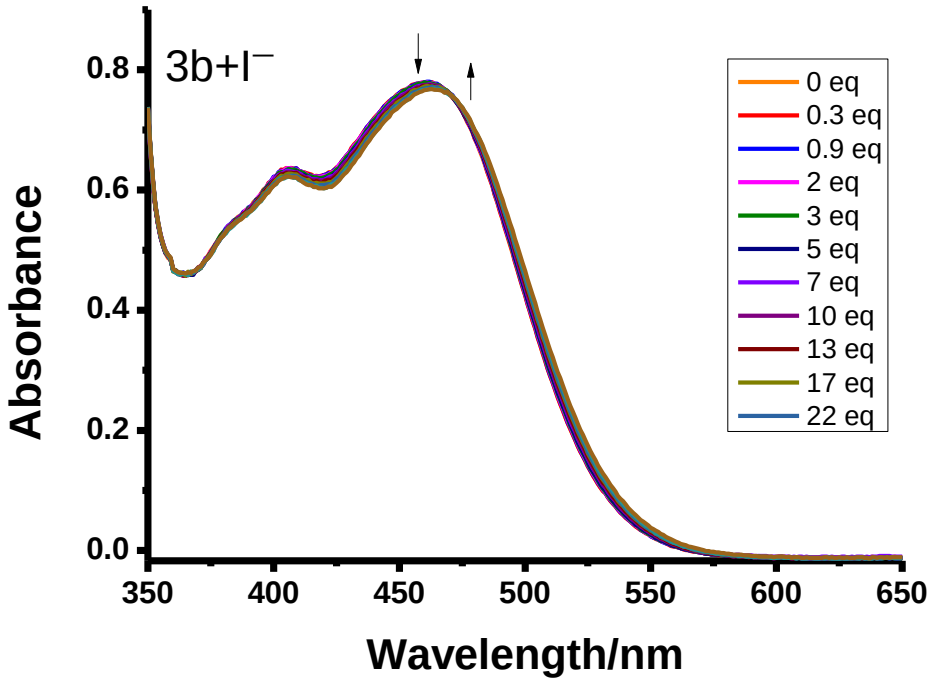

(b)

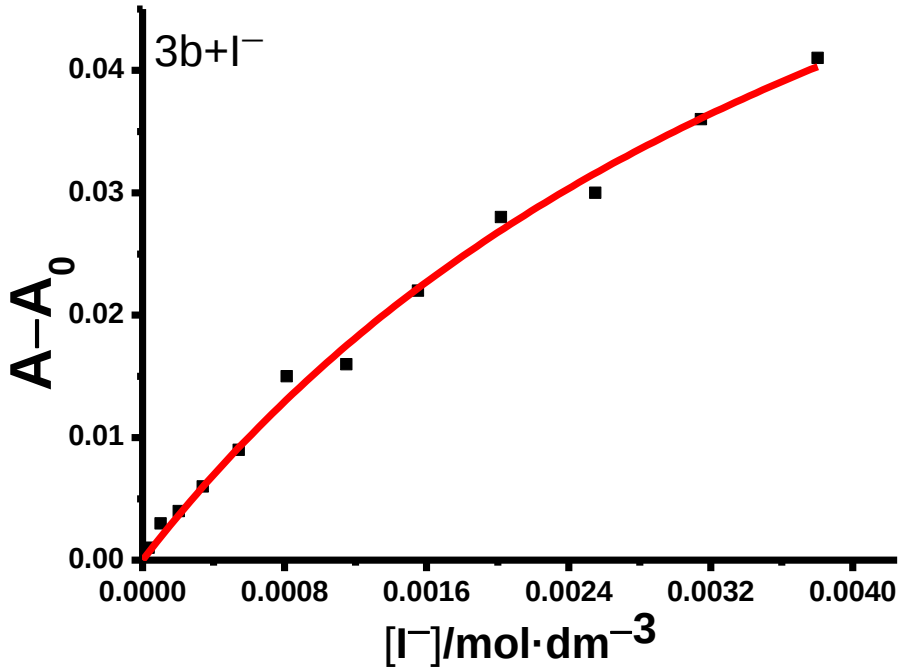

Figure S23. (a) UV–vis spectral changes of **3b** (1.2×10^{-4} mol·dm^{-3}) in CH_3CN upon addition of I^-. (b) A plot of the absorbance change at 500 nm as a function of the concentration of I^- and its theoretical fit for the 1:1 binding of complex **3b** with I^-.

(a)

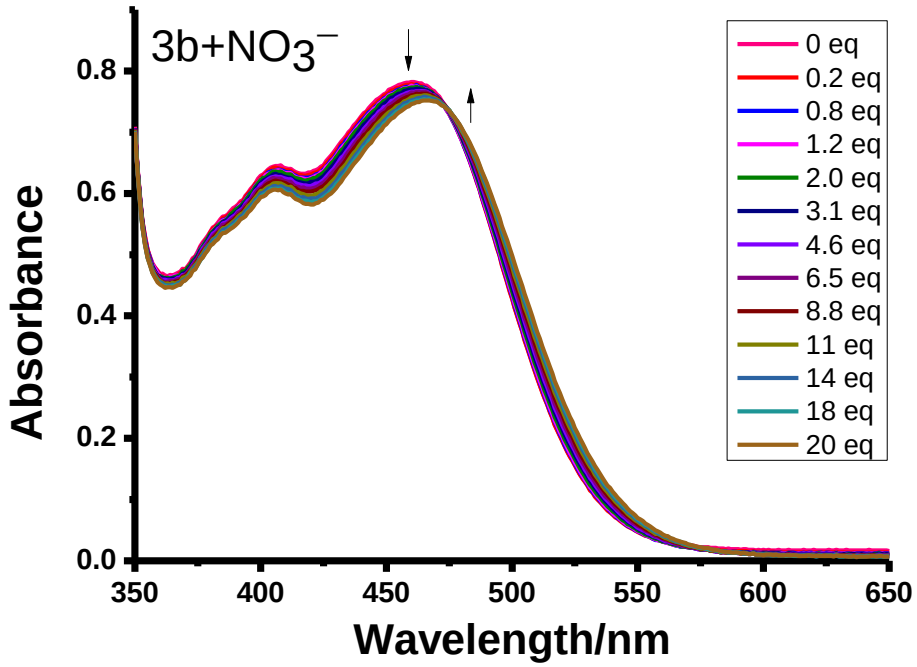

(b)

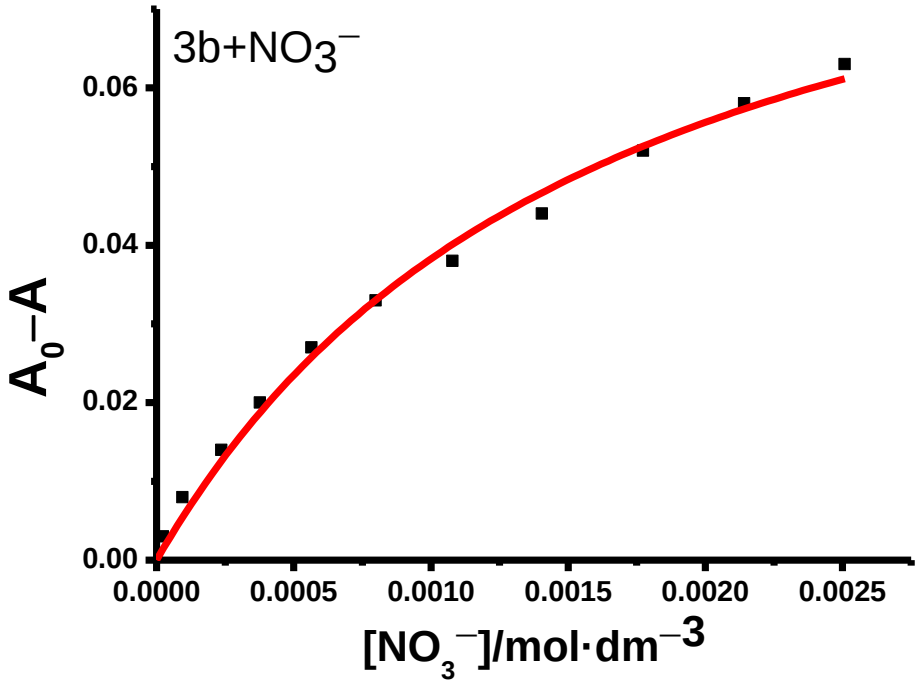

Figure S24. (a) UV–vis spectral changes of **3b** (1.2×10^{-4} mol·dm^{-3}) in CH_3CN upon addition of NO_3^-. (b) A plot of the absorbance change at 440 nm as a function of the concentration of NO_3^- and its theoretical fit for the 1:1 binding of complex **3b** with NO_3^-.

(a)

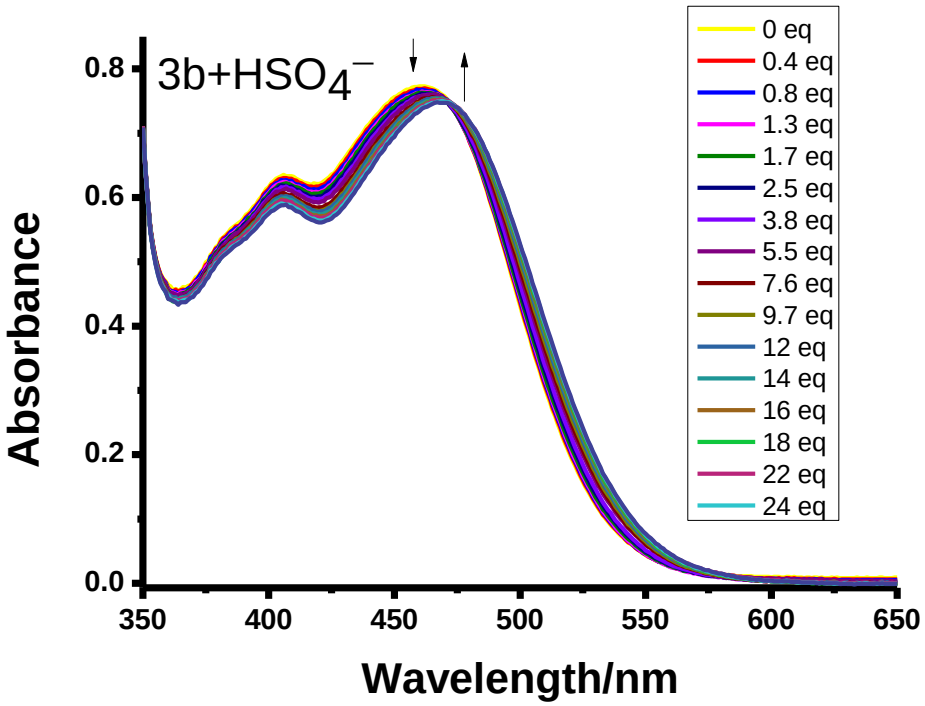

(b)

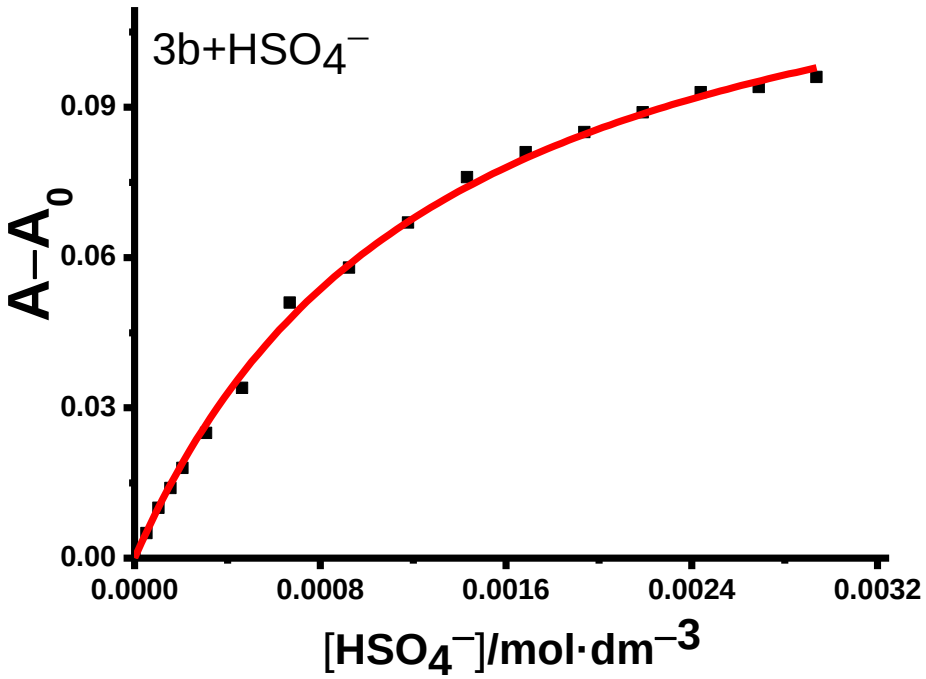

Figure S25. (a) UV–vis spectral changes of **3b** (1.2×10^{-4} mol·dm^{-3}) in CH_3CN upon addition of HSO_4^-. (b) A plot of the absorbance change at 500 nm as a function of the concentration of HSO_4^- and its theoretical fit for the 1:1 binding of complex **3b** with HSO_4^-.

(a)

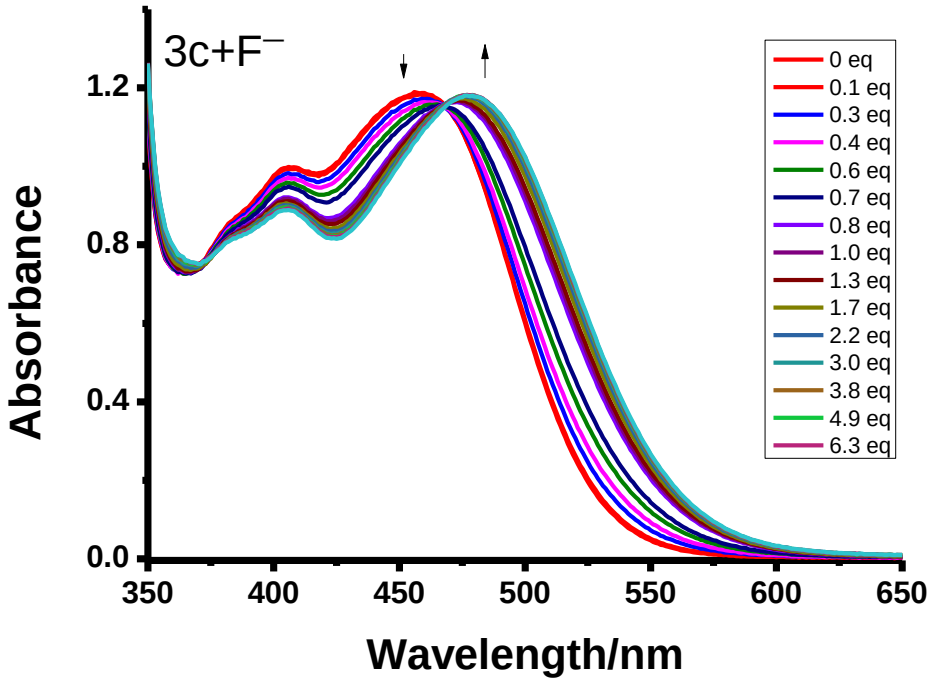

(b)

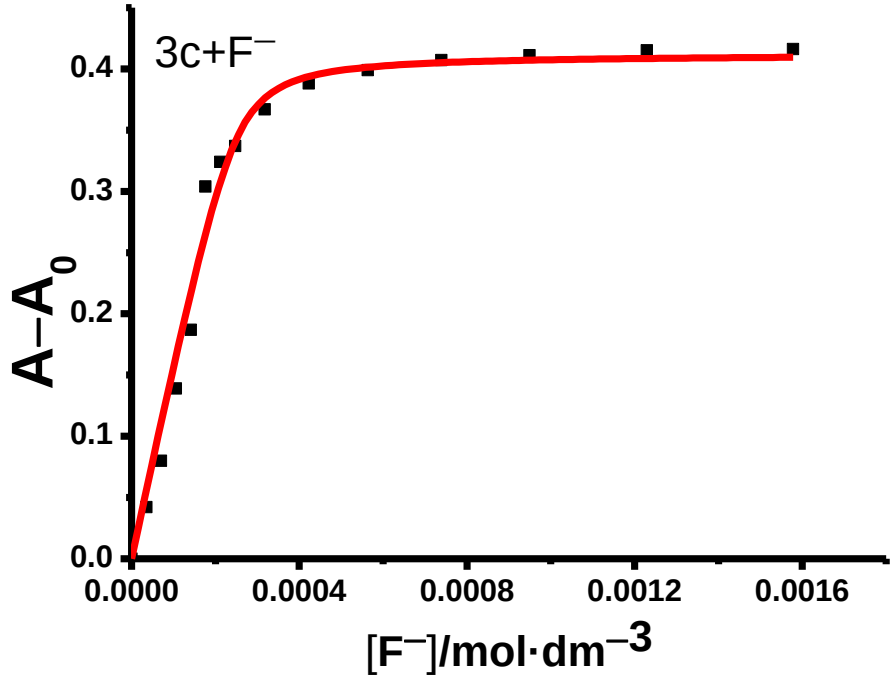

Figure S26. (a) UV–vis spectral changes of **3c** (2.5×10^{-4} mol·dm^{-3}) in CH_3CN upon addition of F^-. (b) A plot of the absorbance change at 500 nm as a function of the concentration of F^- and its theoretical fit for the 1:1 binding of complex **3c** with F^-.

(a)

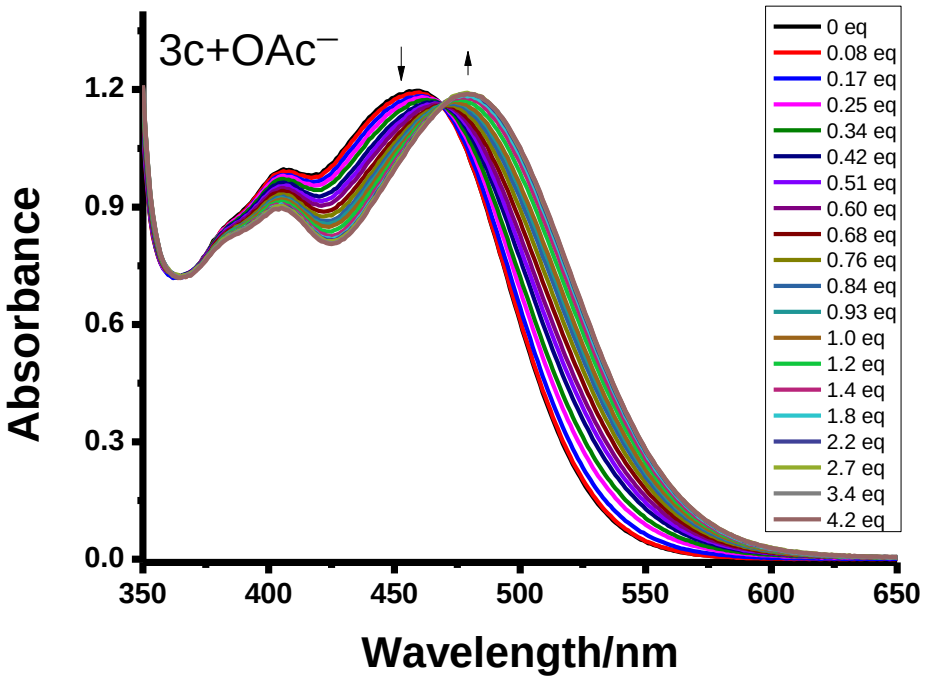

(b)

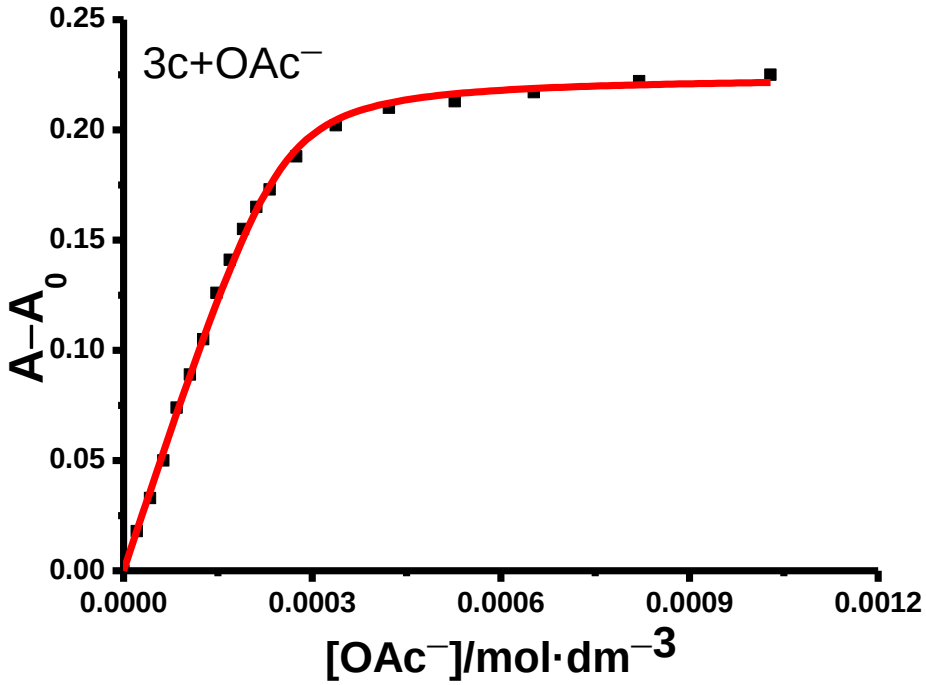

Figure S27. (a) UV–vis spectral changes of **3c** (2.5×10^{-4} mol·dm^{-3}) in CH_3CN upon addition of OAc^-. (b) A plot of the absorbance change at 430 nm as a function of the concentration of OAc^- and its theoretical fit for the 1:1 binding of complex **3c** with OAc^-.

(a)

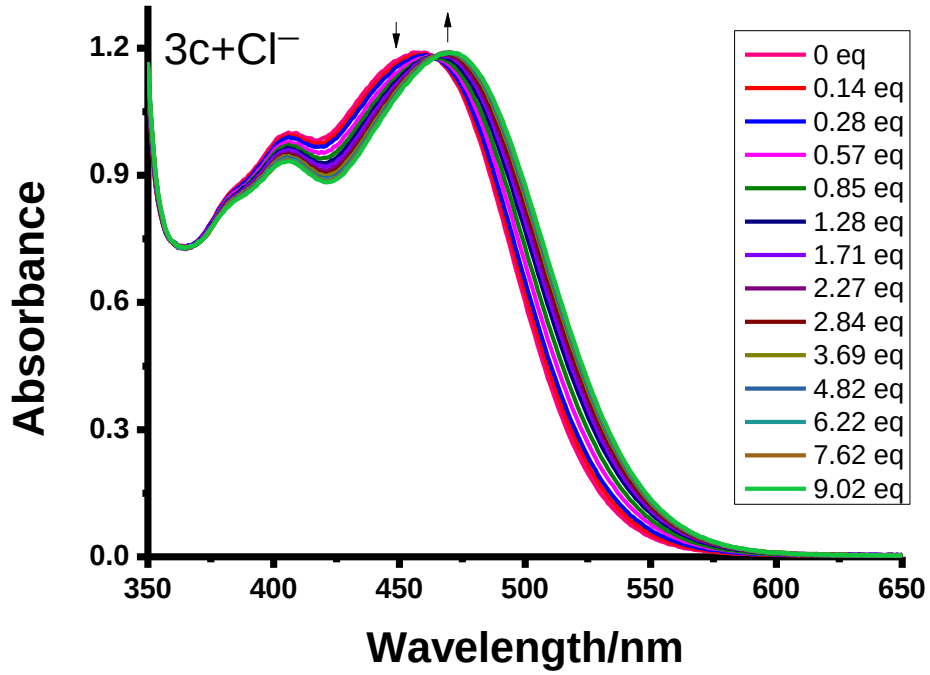

(b)

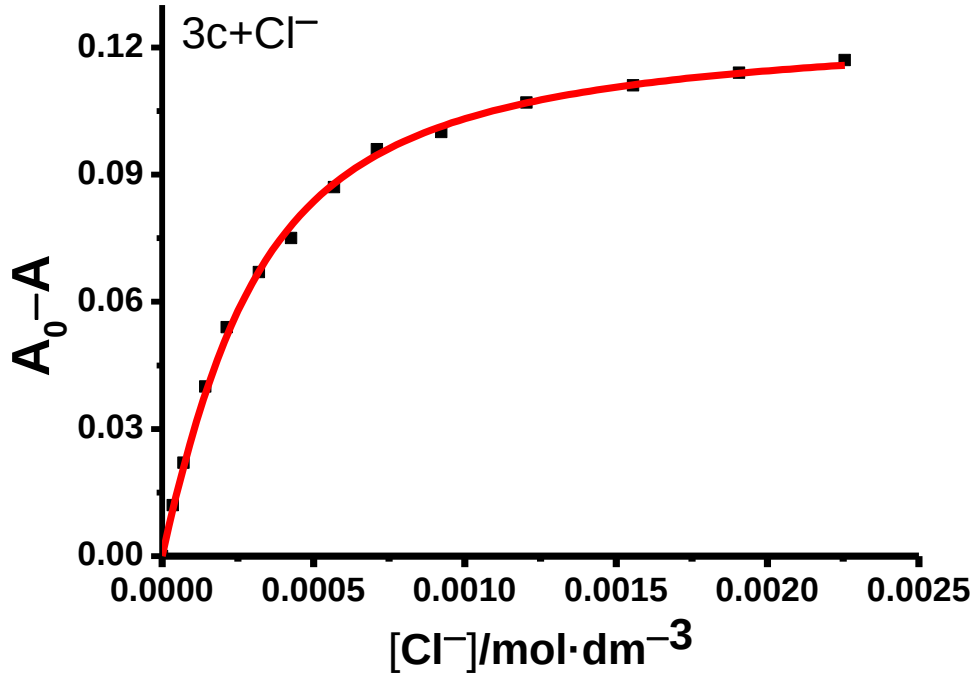

Figure S28. (a) UV–vis spectral changes of **3c** (2.5×10^{-4} mol·dm^{-3}) in CH_3CN upon addition of Cl^-. (b) A plot of the absorbance change at 440 nm as a function of the concentration of Cl^- and its theoretical fit for the 1:1 binding of complex **3c** with Cl^-.

(a)

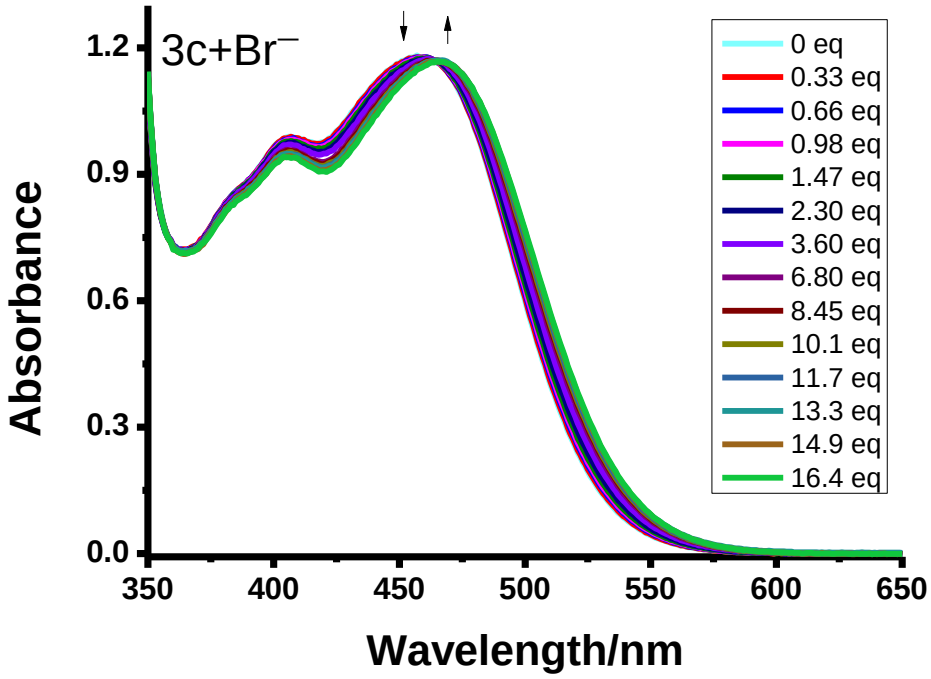

(b)

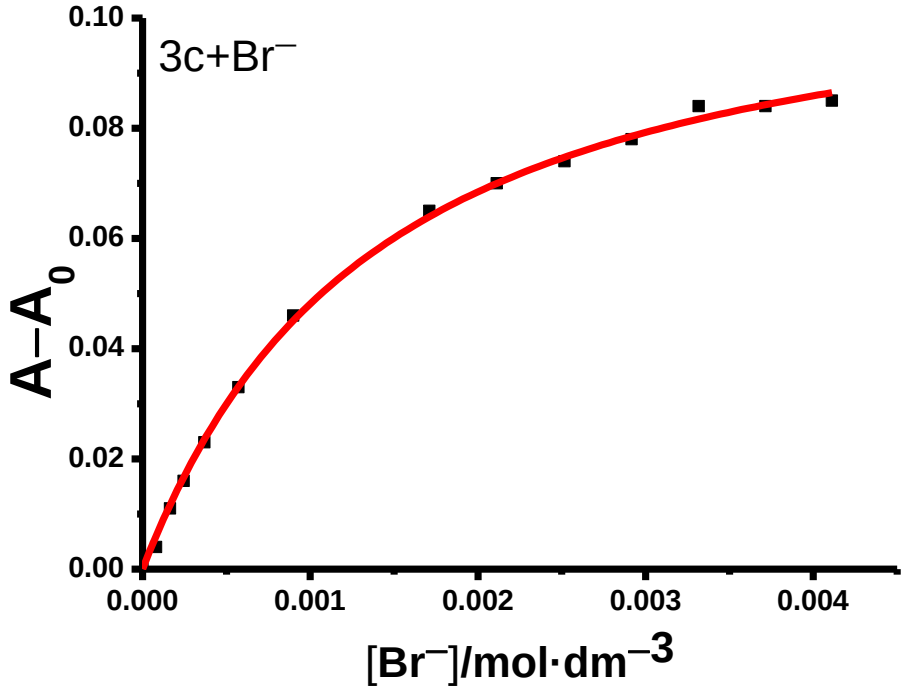

Figure S29. (a) UV–vis spectral changes of **3c** (2.5×10^{-4} mol·dm^{-3}) in CH_3CN upon addition of Br^-. (b) A plot of the absorbance change at 480 nm as a function of the concentration of Br^- and its theoretical fit for the 1:1 binding of complex **3c** with Br^-.

(a)

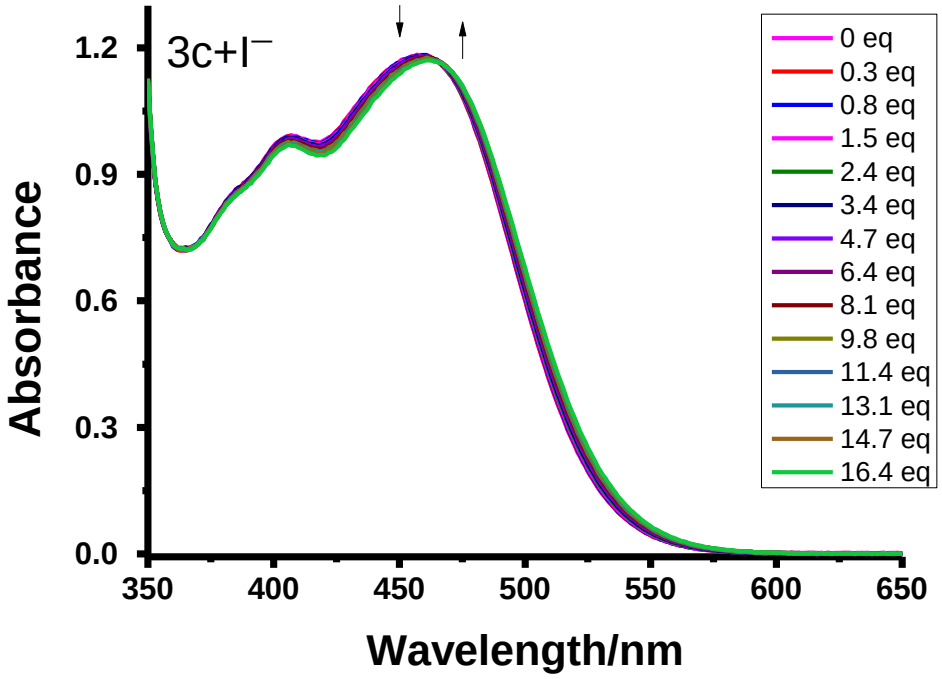

(b)

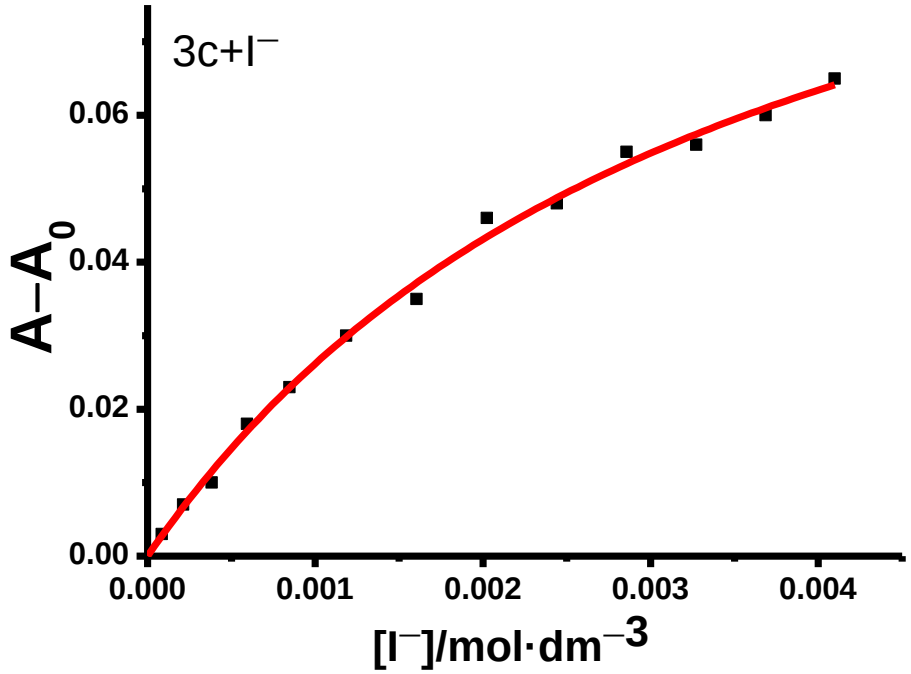

Figure S30. (a) UV–vis spectral changes of **3c** (2.5×10^{-4} mol·dm^{-3}) in CH_3CN upon addition of I^-. (b) A plot of the absorbance change at 490 nm as a function of the concentration of I^- and its theoretical fit for the 1:1 binding of complex **3c** with I^-.

(a)

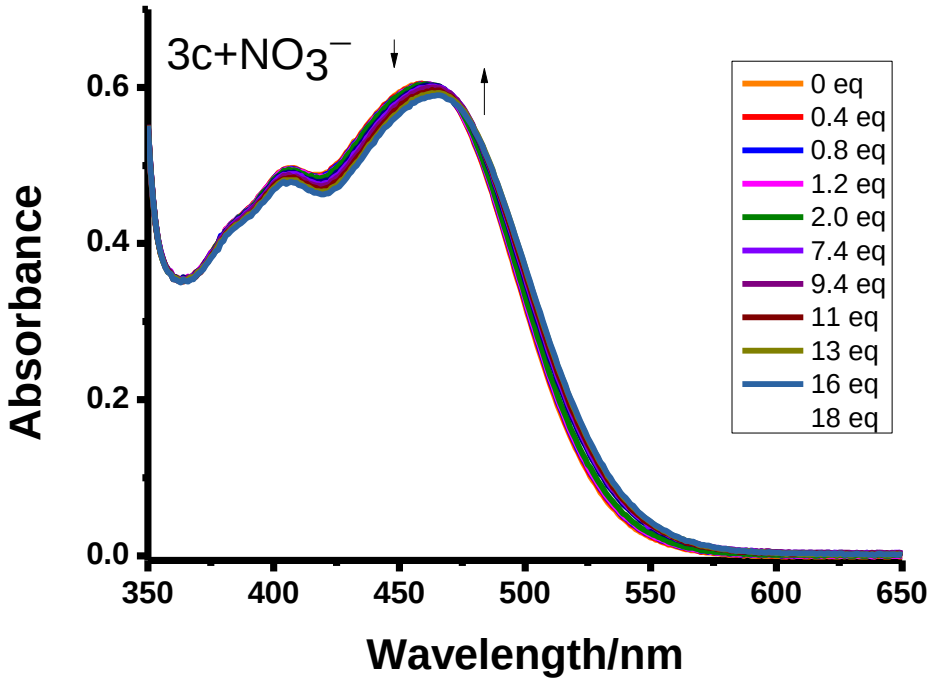

(b)

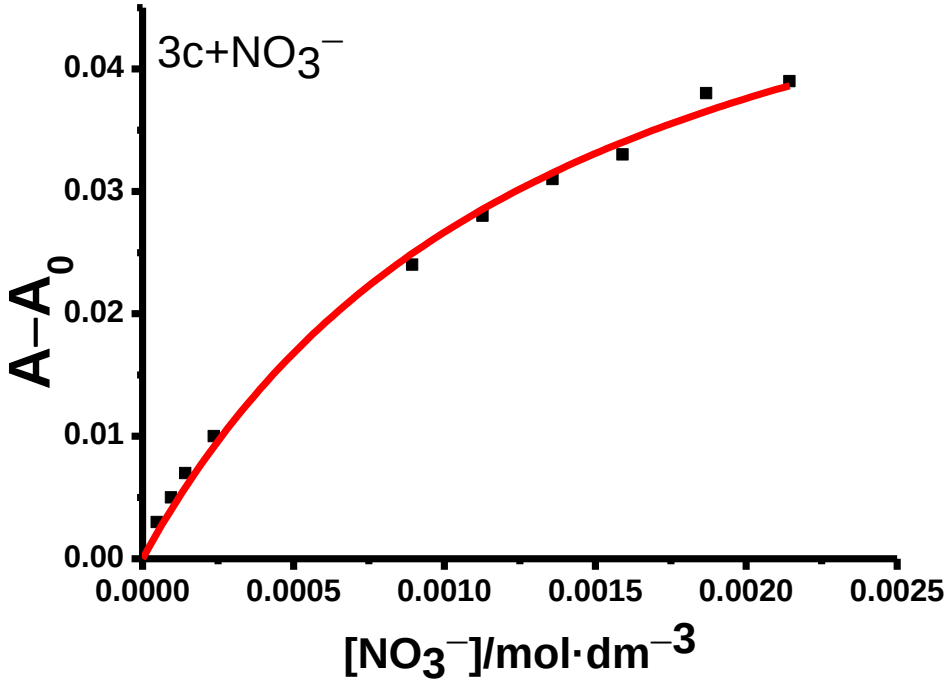

Figure S31. (a) UV–vis spectral changes of **3c** (2.5×10^{-4} mol·dm^{-3}) in CH_3CN upon addition of NO_3^-. (b) A plot of the absorbance change at 530 nm as a function of the concentration of NO_3^- and its theoretical fit for the 1:1 binding of complex **3c** with NO_3^-.

(a)

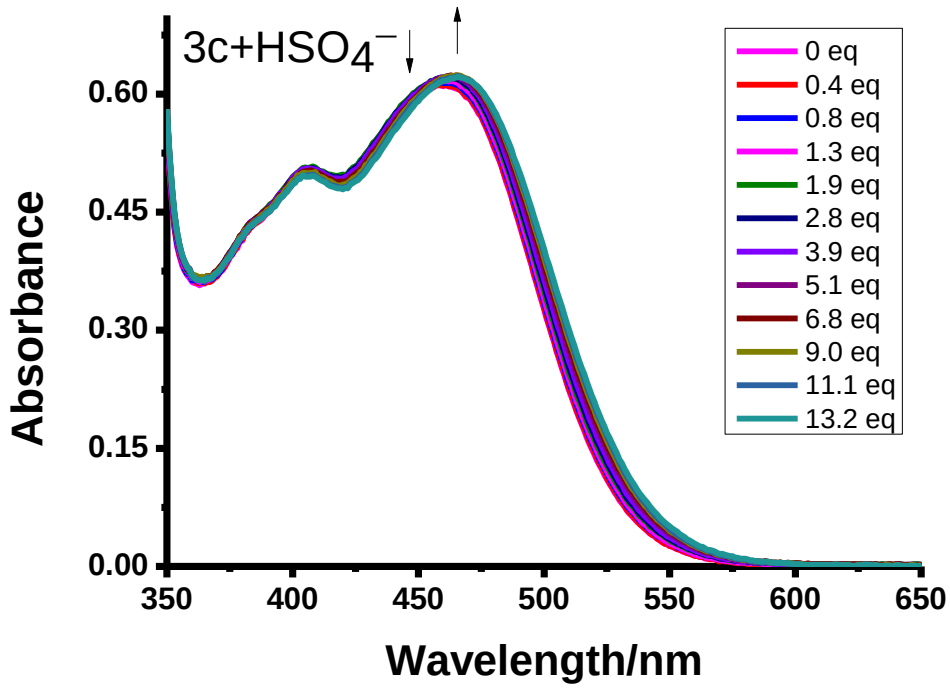

(b)

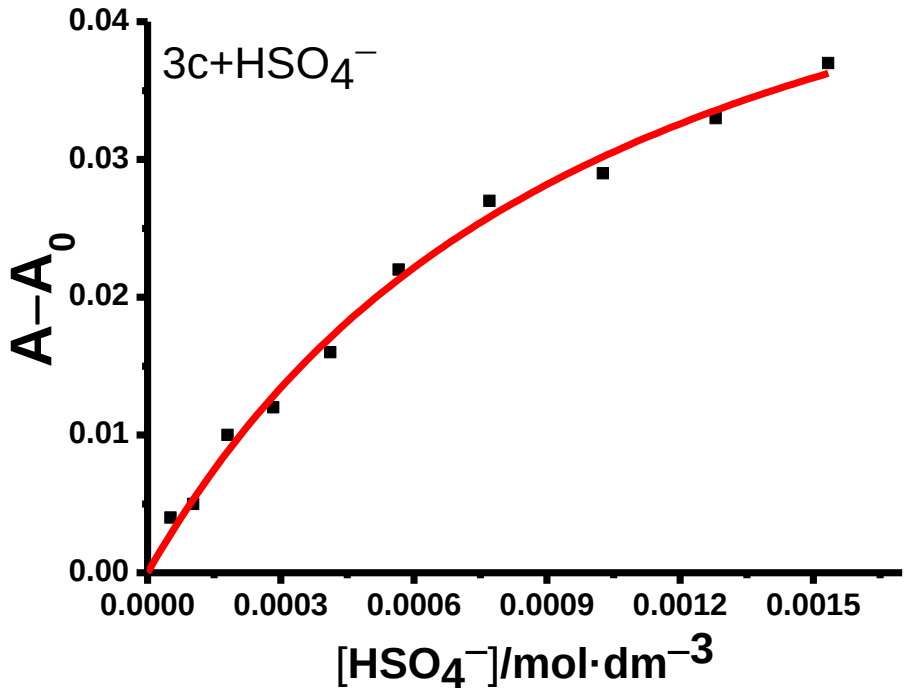

Figure S32. (a) UV–vis spectral changes of **3c** (2.5×10^{-4} mol·dm^{-3}) in CH_3CN upon addition of HSO_4^-. (b) A plot of the absorbance change at 540 nm as a function of the concentration of HSO_4^- and its theoretical fit for the 1:1 binding of complex **3c** with HSO_4^-.

(a)

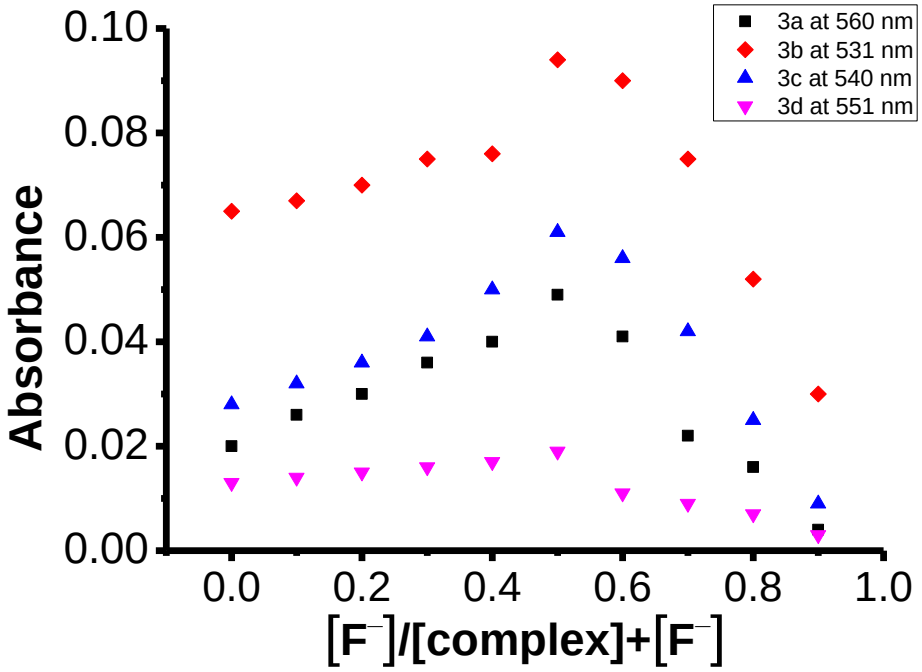

(b)

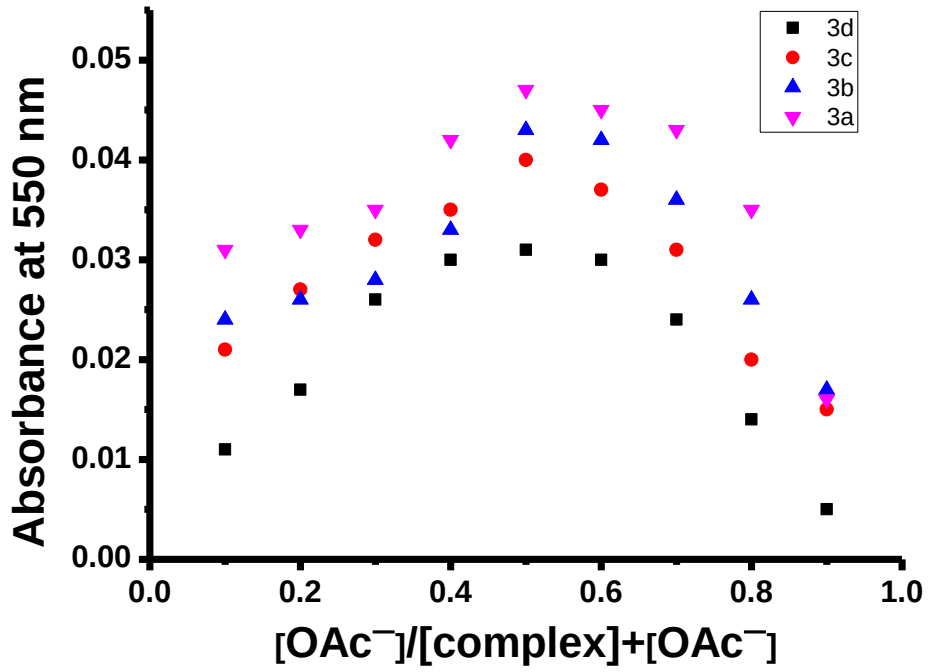

Figure S33. (a) Job's plots of complexes **3a**–**3c** with F^- in CH_3CN ([complex] + [F^-] = 1×10^{-4} mol·dm^{-3}) ; (b) Job's plots of complexes **3a**–**3d** with OAc^- in CH_3CN ([complex] + [OAc^-] = 1×10^{-4} mol·dm^{-3})

(a)

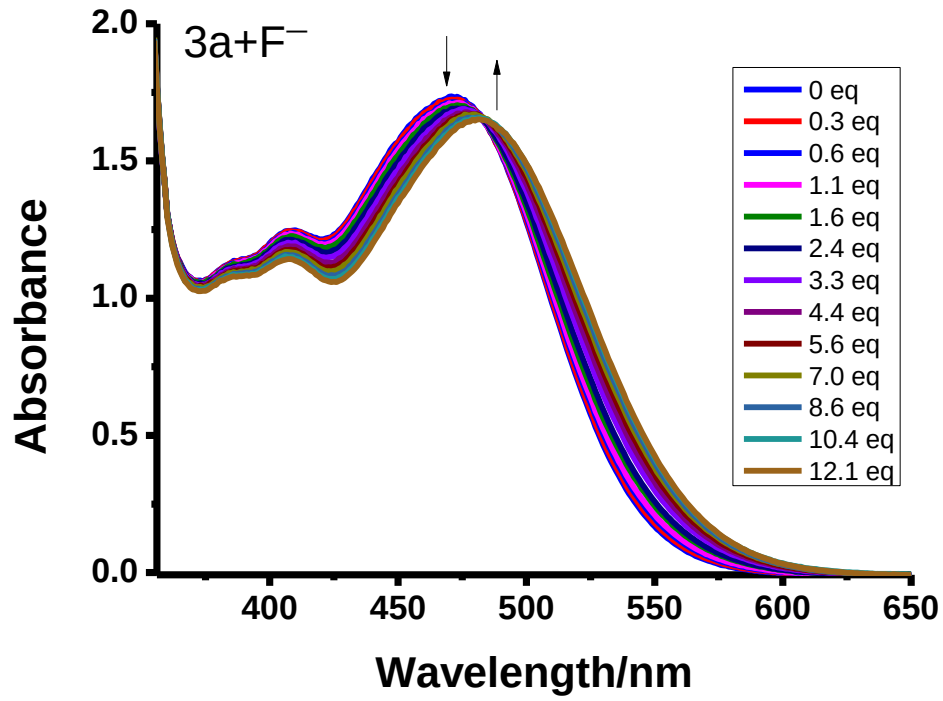

(b)

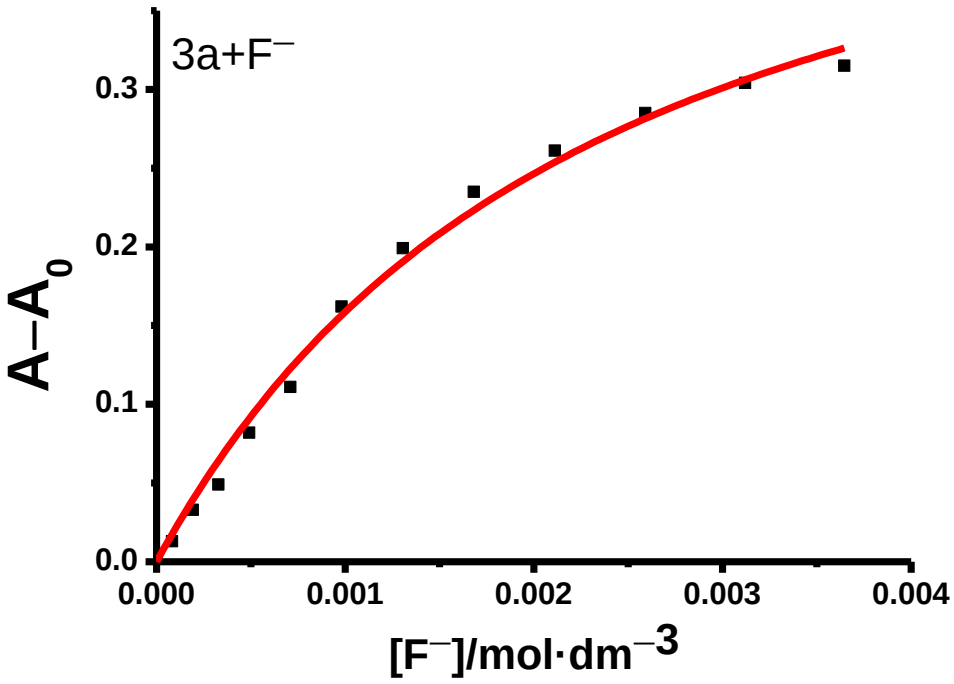

Figure S34. (a) UV–vis spectral changes of **3a** (3×10^{-4} mol·dm^{-3}) in DMSO upon addition of F^-. (b) A plot of the absorbance change at 510 nm as a function of the concentration of F^- and its theoretical fit for the 1:1 binding of complex **3a** with F^-.

(a)

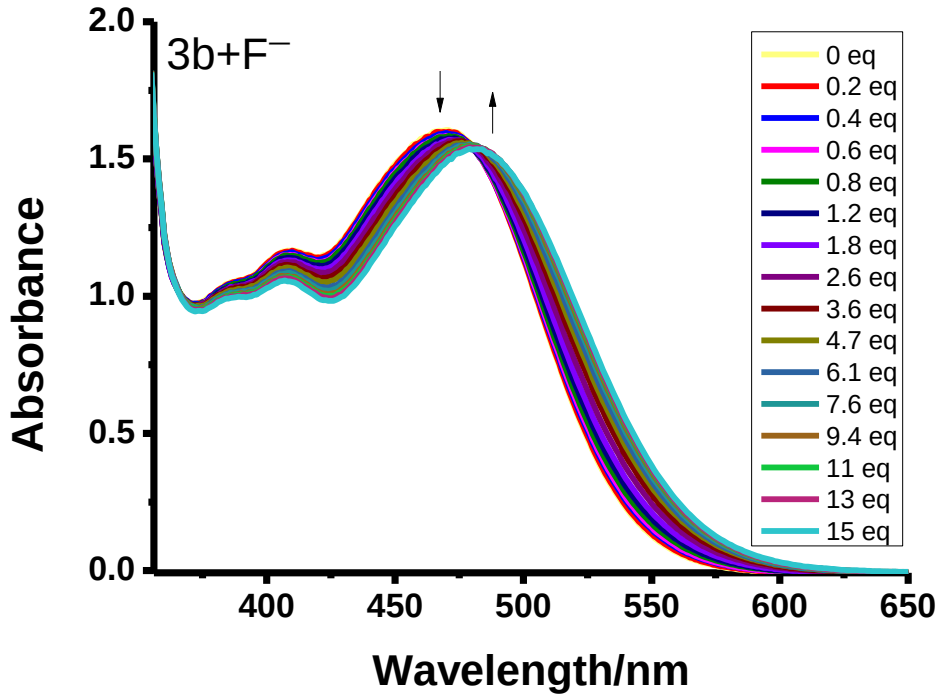

(b)

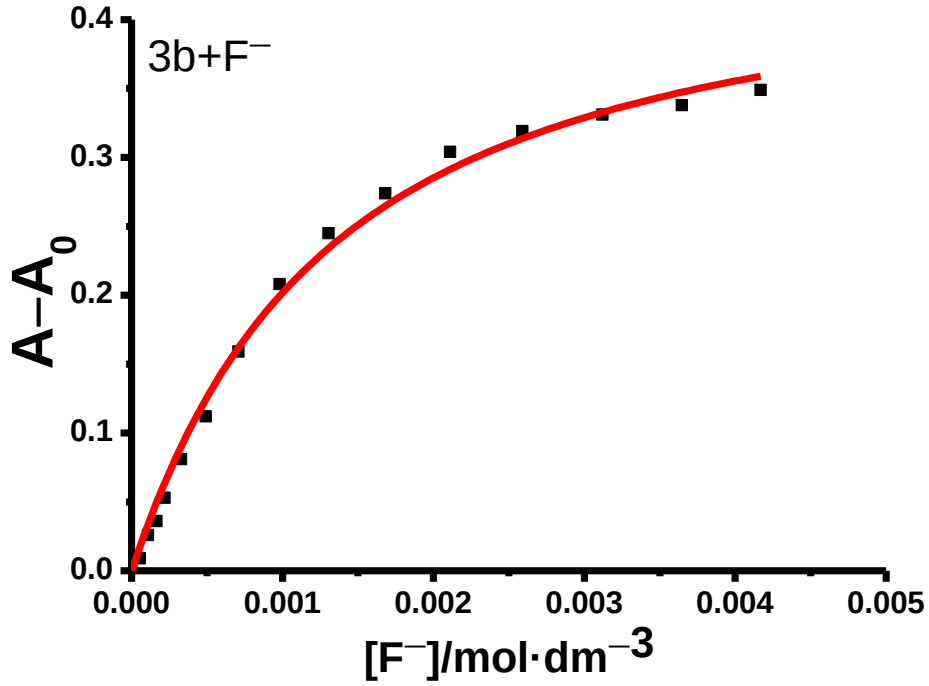

Figure S35. (a) UV–vis spectral changes of **3b** (2.76×10^{-4} mol·dm^{-3}) in DMSO upon addition of F^-. (b) A plot of the absorbance change at 510 nm as a function of the concentration of F^- and its theoretical fit for the 1:1 binding of complex **3b** with F^-.

(a)

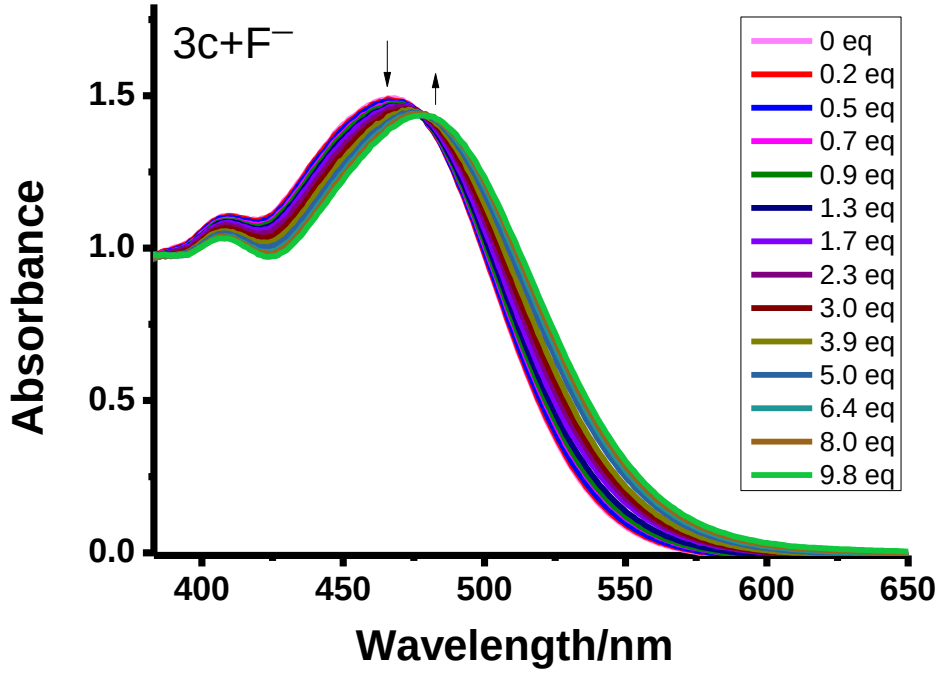

(b)

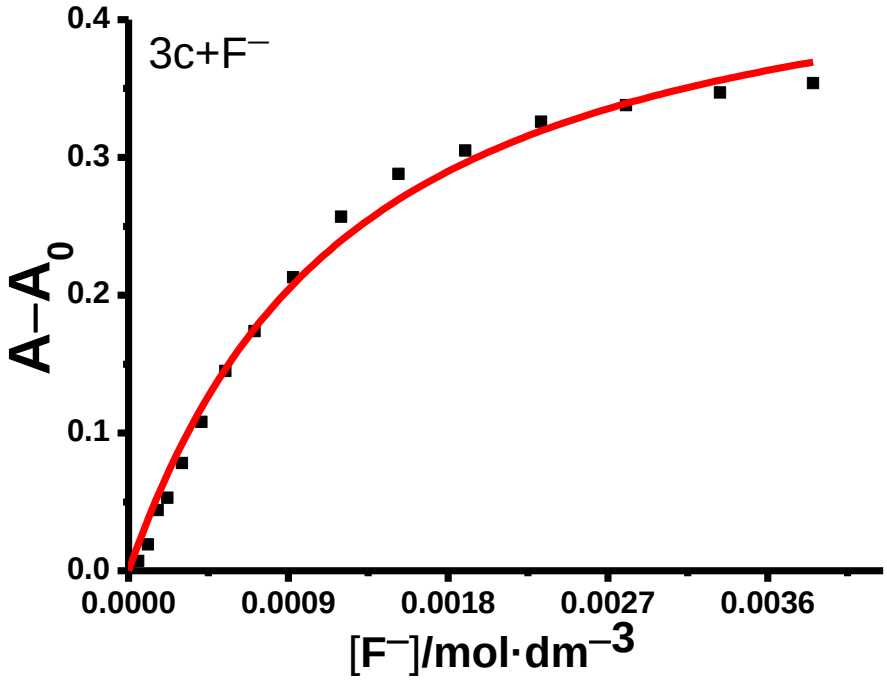

Figure S36. (a) UV–vis spectral changes of **3c** (2.38×10^{-4} mol·dm^{-3}) in DMSO upon addition of F^-. (b) A plot of the absorbance change at 510 nm as a function of the concentration of F^- and its theoretical fit for the 1:1 binding of complex **3c** with F^-.

Table S5 Binding constants (log *K*) of **3a**–**3d** with anions in DMSO[a]

Complex	F^-	OAc^-	Cl^-	Br^-	NO_3^-	HSO_4^-
3a	2.68±0.12	2.85±0.11	[b]	[b]	[b]	[b]
3b	2.94±0.09	3.25±0.11	[b]	[b]	[b]	[b]
3c	2.97±0.10	3.38±0.16	[b]	[b]	[b]	[b]
3d	[c]	3.87±0.06	[b]	[b]	[b]	[b]

[a]Binding constants were determined by 1:1 model using nonlinear fitting methods. [b]Spectral changes were not suitable for accurate measurement of binding constant. [c]Deprotonation occurred.

(a)

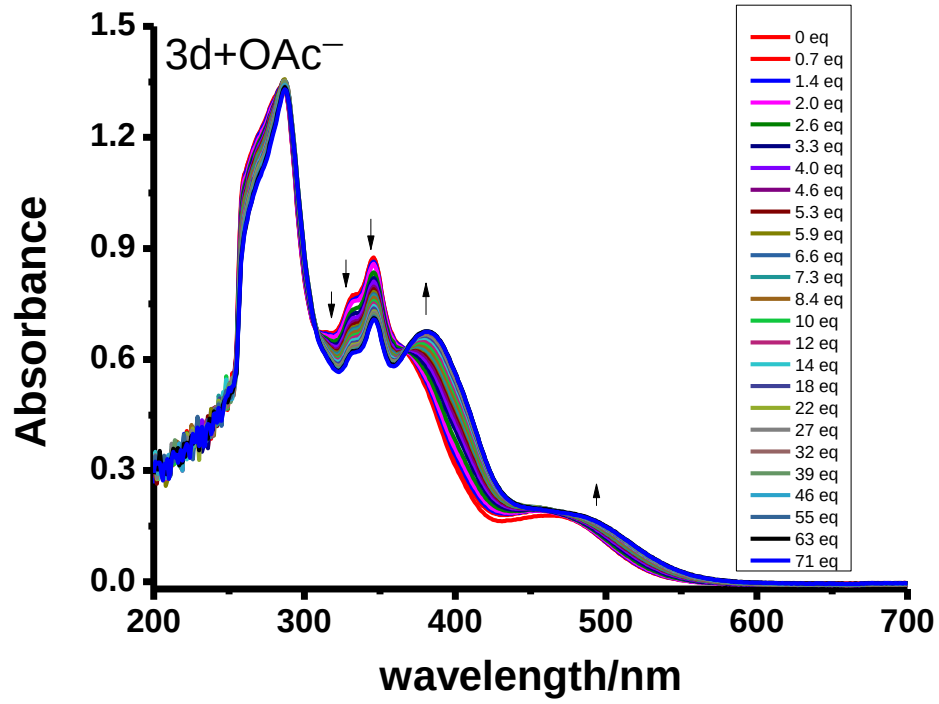

(b)

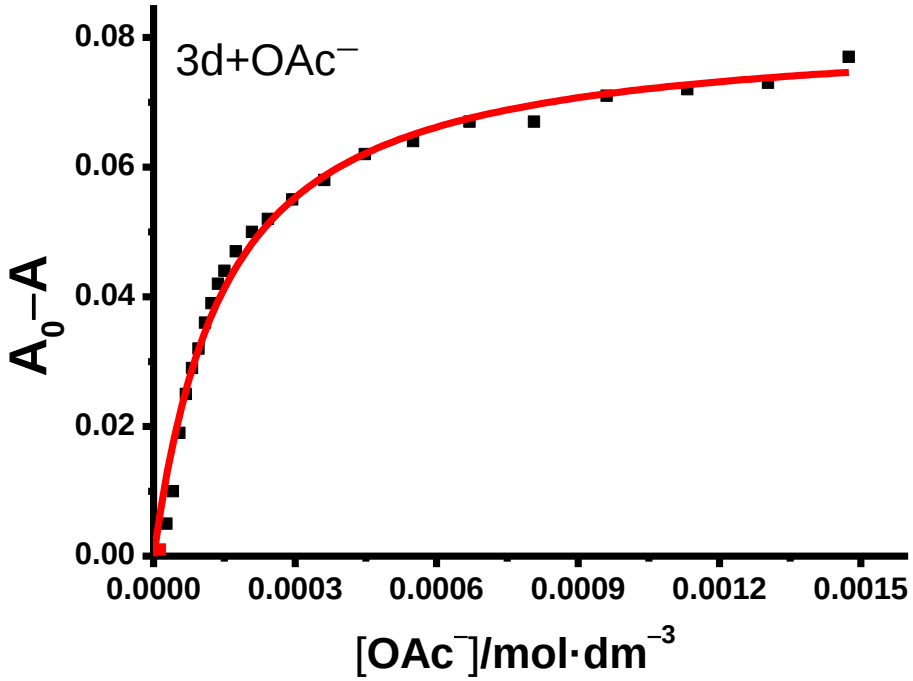

Figure S37. (a) UV–vis spectral changes of **3d** (2.1×10^{-5} mol·dm^{-3}) in DMSO upon addition of OAc^-. (b) A plot of the absorbance change at 316 nm as a function of the concentration of OAc^- and its theoretical fit for the 1:1 binding of complex **3d** with OAc^-.

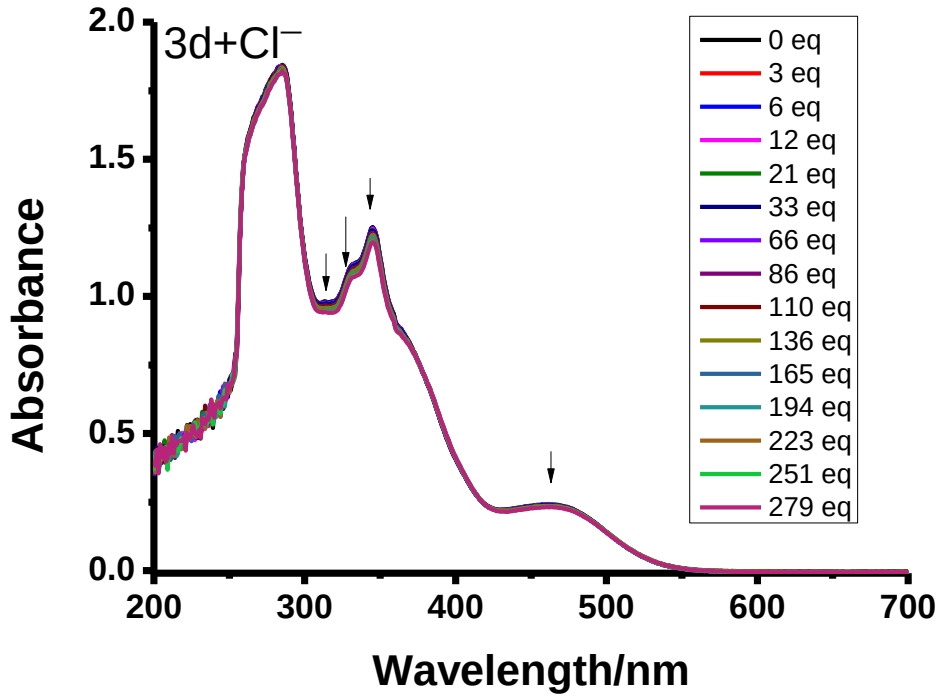

Figure S38. UV–vis spectral changes of **3d** (2.81×10^{-4} mol·dm^{-3}) in DMSO upon addition of Cl^-.

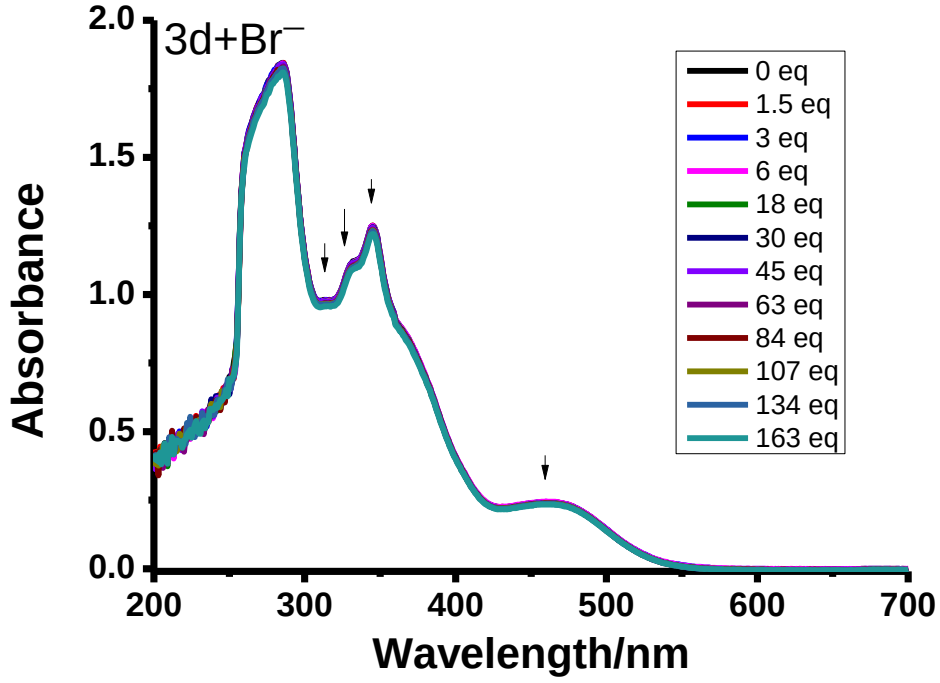

Figure S39. UV–vis spectral changes of **3d** (2.81×10^{-4} mol·dm^{-3}) in DMSO upon addition of Br^-.

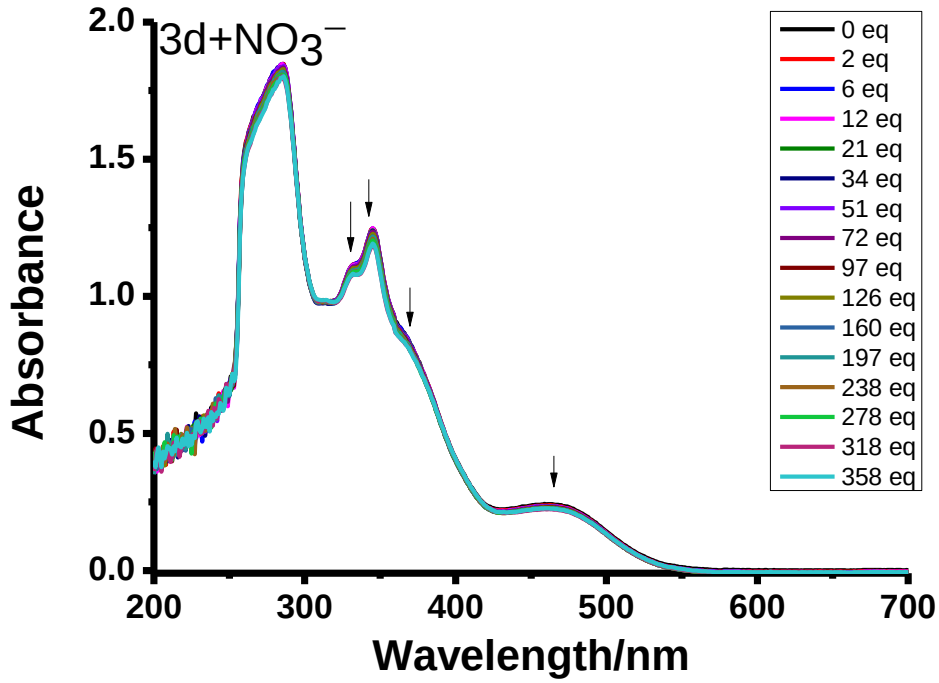

Figure S40. UV–vis spectral changes of **3d** (2.81 × 10^{-4} mol·dm^{-3}) in DMSO upon addition of NO_3^-.

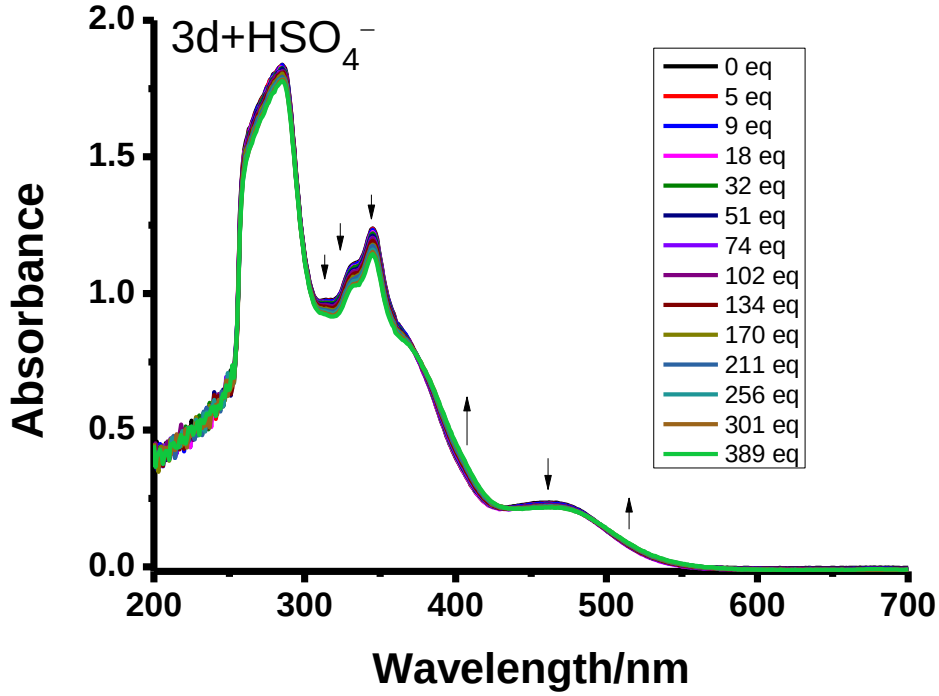

Figure S41. UV–vis spectral changes of **3d** (2.81 × 10^{-4} mol·dm^{-3}) in DMSO upon addition of HSO_4^-.

(a)

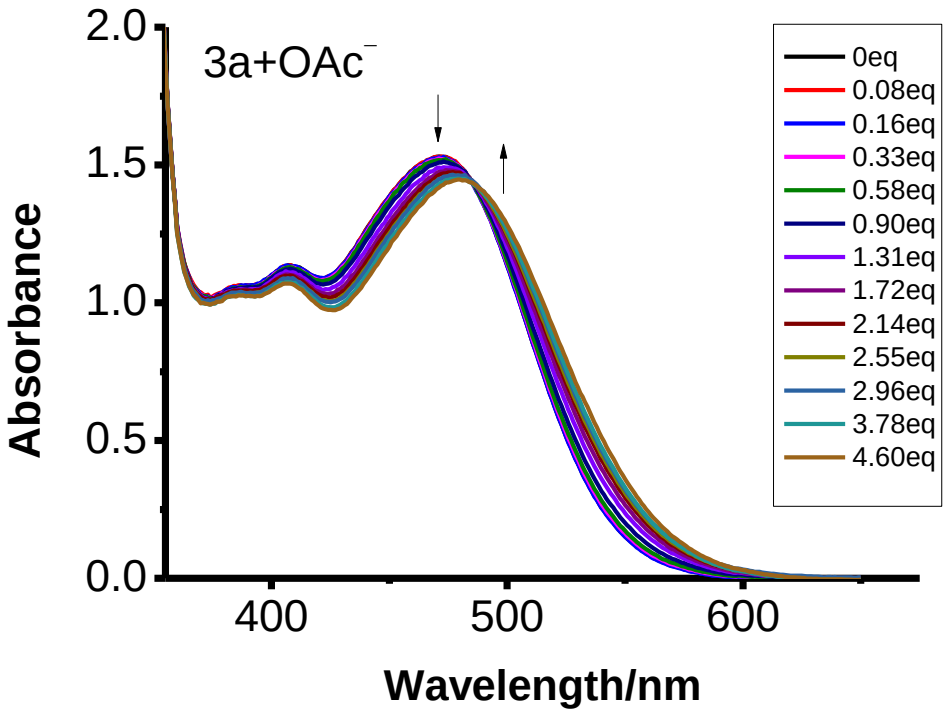

(b)

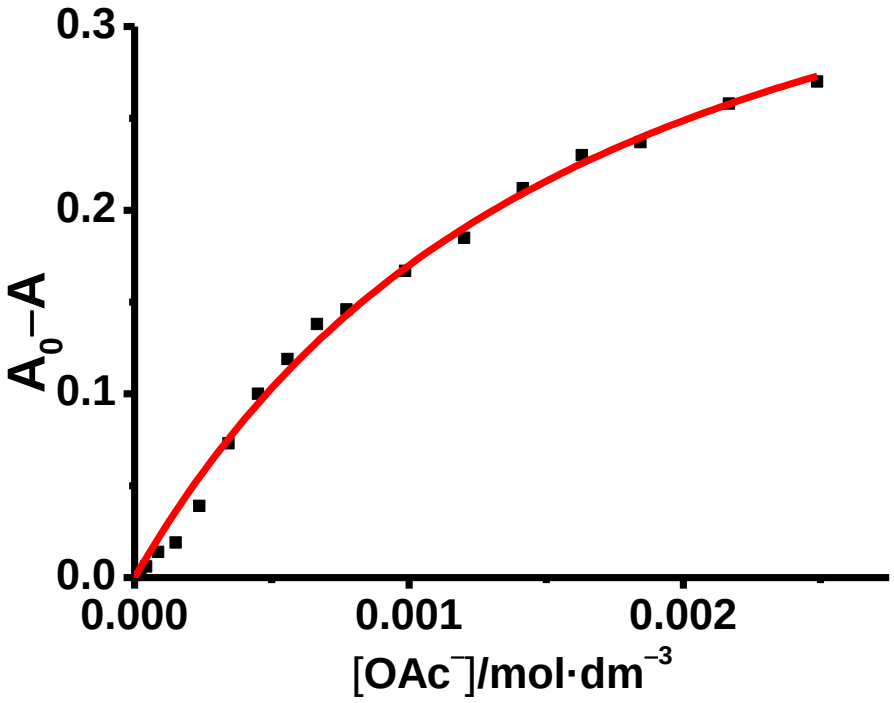

Figure S42. (a) UV–vis spectral changes of **3a** (3×10^{-4} mol·dm^{-3}) in DMSO upon addition of OAc^-. (b) A plot of the absorbance change at 440 nm as a function of the concentration of OAc^- and its theoretical fit for the 1:1 binding of complex **3a** with OAc^-.

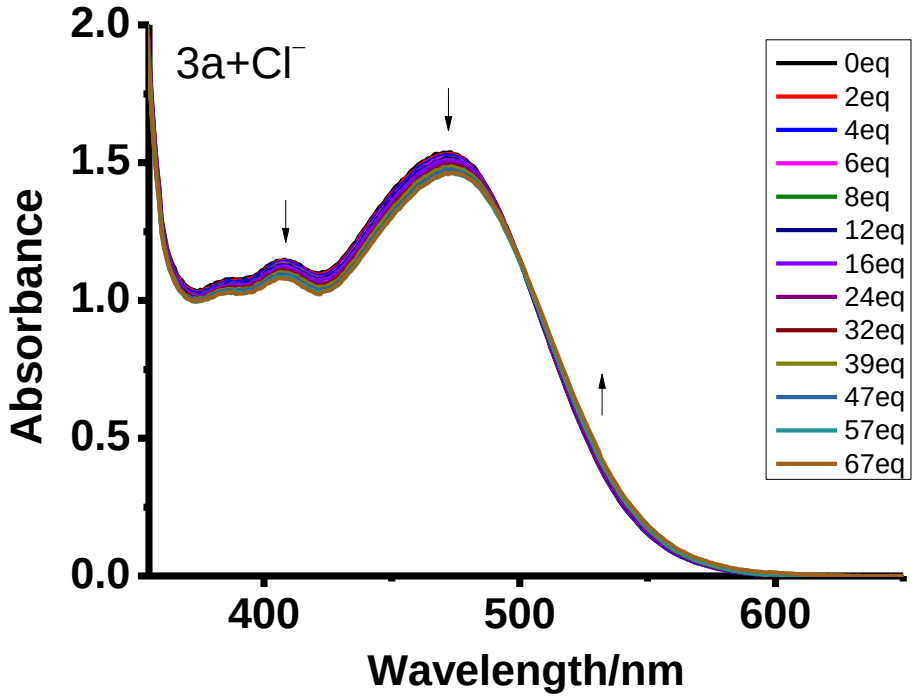

Figure S43. UV–vis spectral changes of **3a** (3×10^{-4} mol·dm^{-3}) in DMSO upon addition of Cl^-.

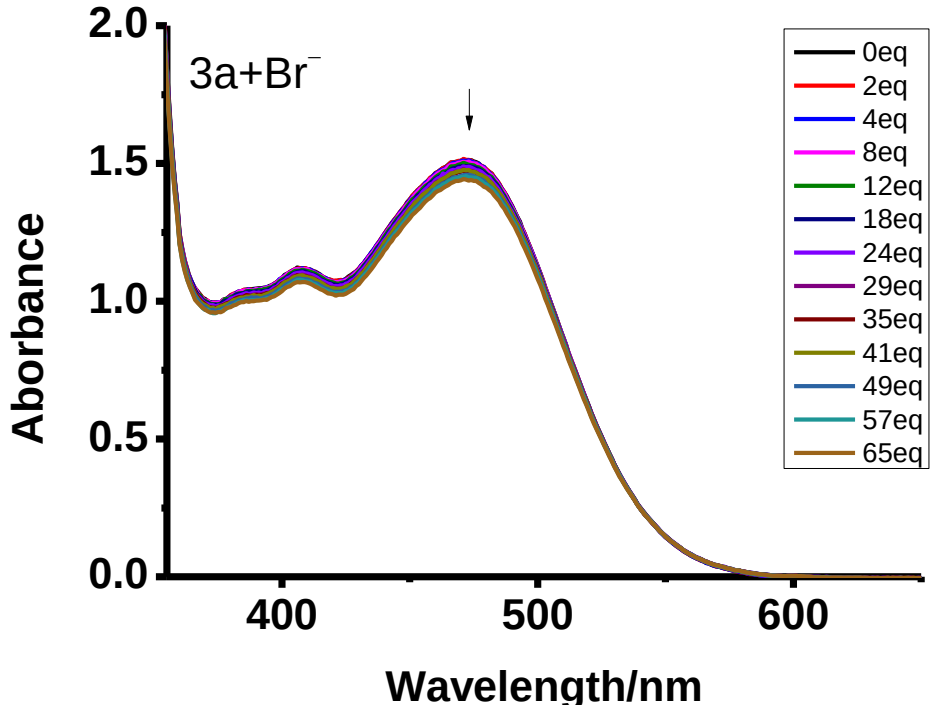

Figure S44. UV–vis spectral changes of **3a** (3×10^{-4} mol·dm^{-3}) in DMSO upon addition of Br^-.

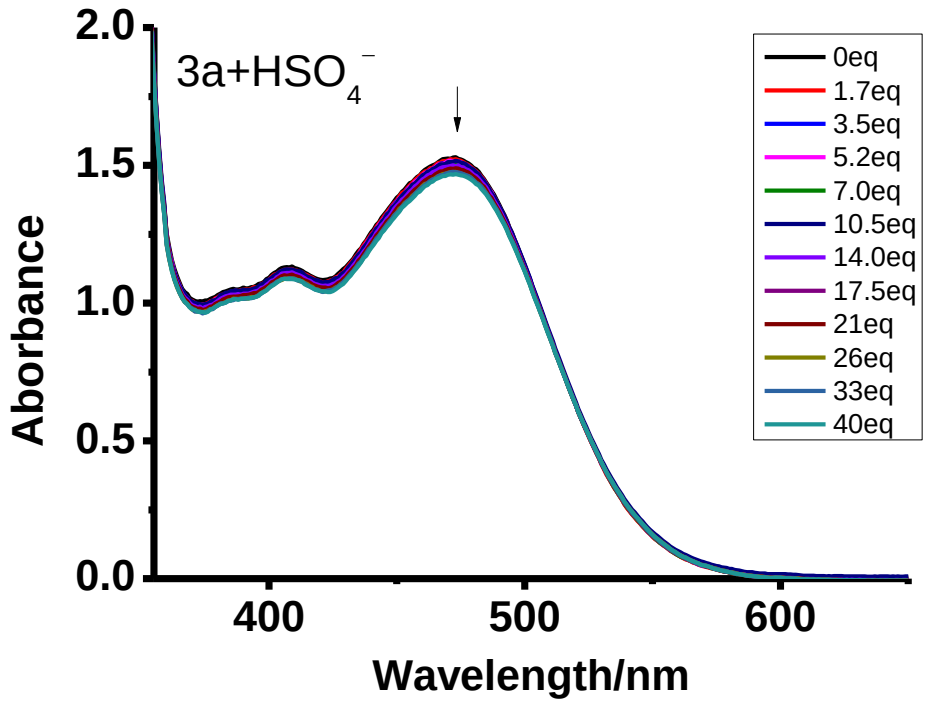

Figure S45. UV–vis spectral changes of **3a** (3×10^{-4} mol·dm^{-3}) in DMSO upon addition of HSO_4^-.

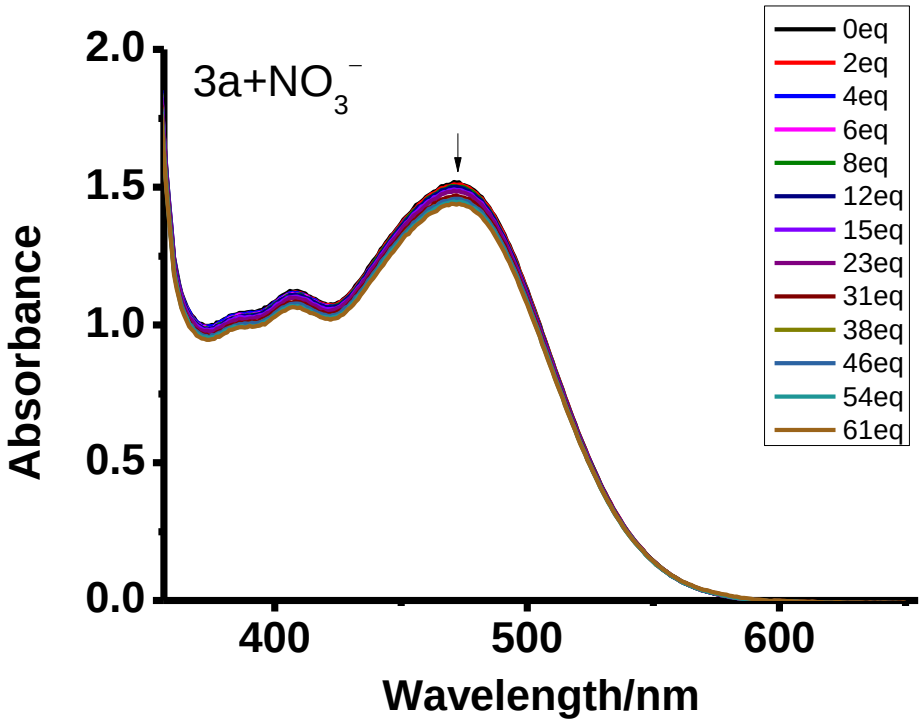

Figure S46. UV–vis spectral changes of **3a** (3×10^{-4} mol·dm^{-3}) in DMSO upon addition of NO_3^-.

(a)

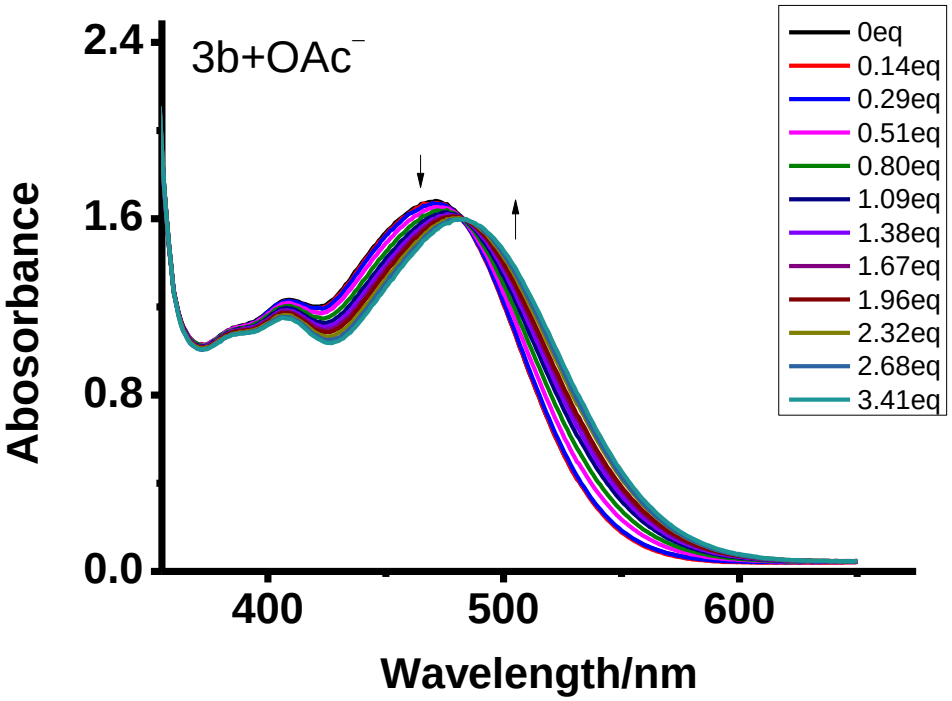

(b)

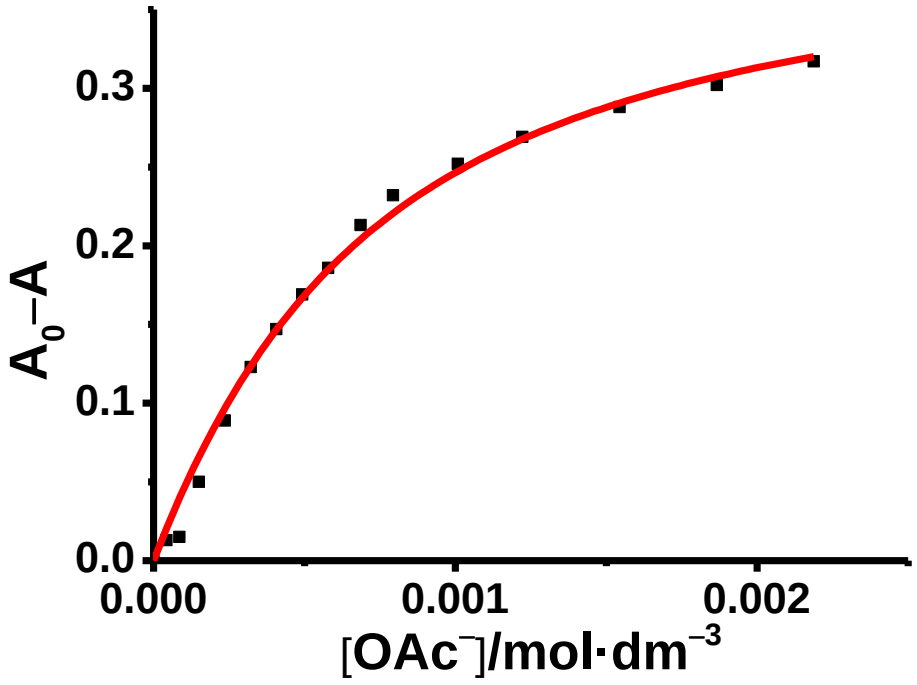

Figure S47. (a) UV–vis spectral changes of **3b** (2.76×10^{-4} mol·dm^{-3}) in DMSO upon addition of OAc^-. (b) A plot of the absorbance change at 449 nm as a function of the concentration of OAc^- and its theoretical fit for the 1:1 binding of complex **3b** with OAc^-.

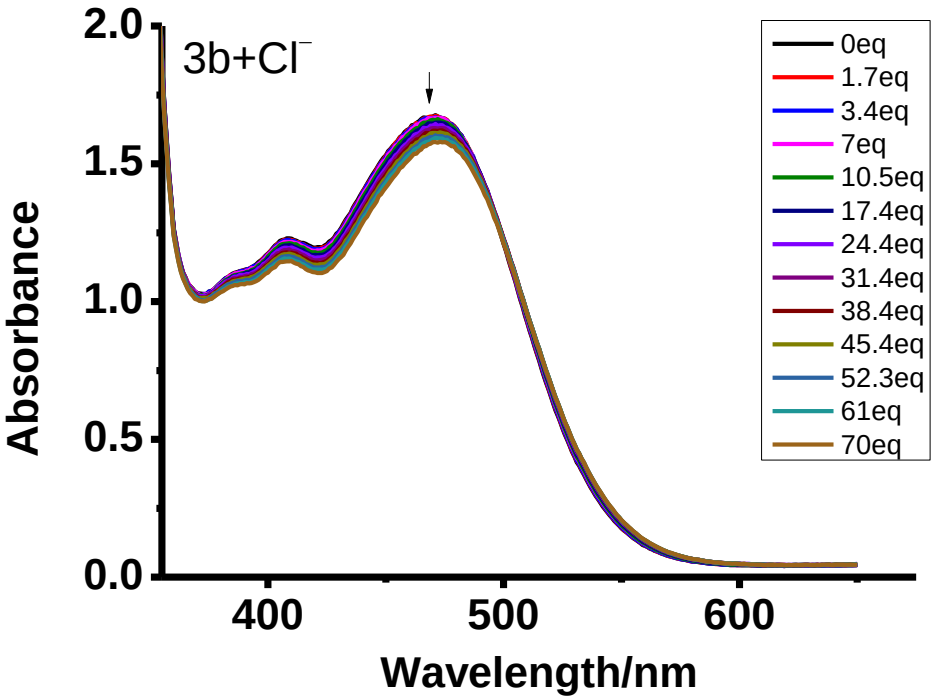

Figure S48. UV–vis spectral changes of **3b** (2.76×10^{-4} mol·dm^{-3}) in DMSO upon addition of Cl^-.

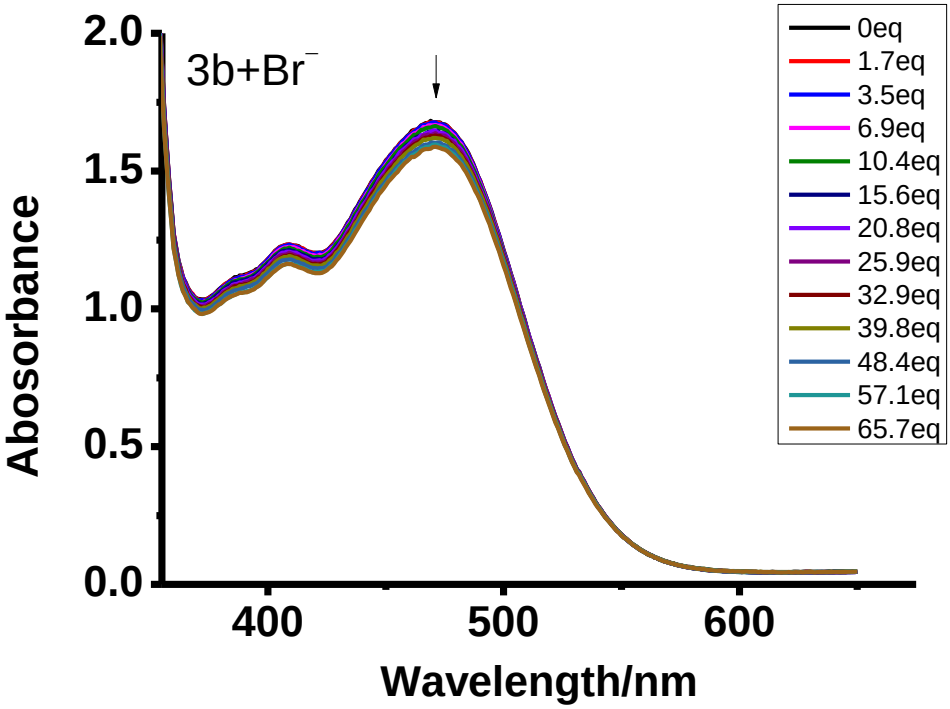

Figure S49. UV–vis spectral changes of **3b** (2.76×10^{-4} mol·dm^{-3}) in DMSO upon addition of Br^-.

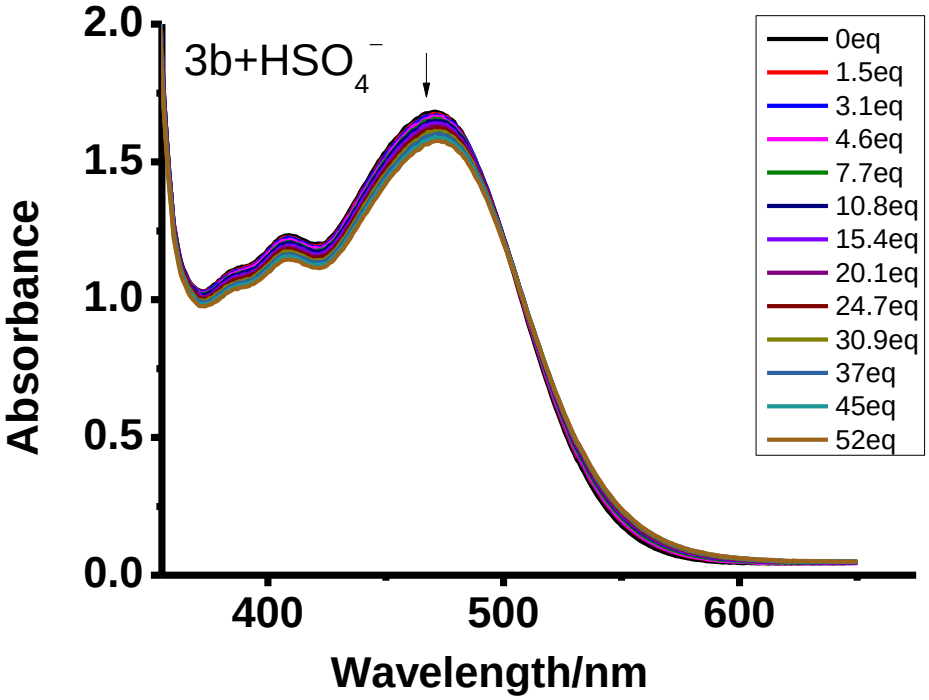

Figure S50. UV–vis spectral changes of **3b** (2.76×10^{-4} mol·dm^{-3}) in DMSO upon addition of HSO_4^-.

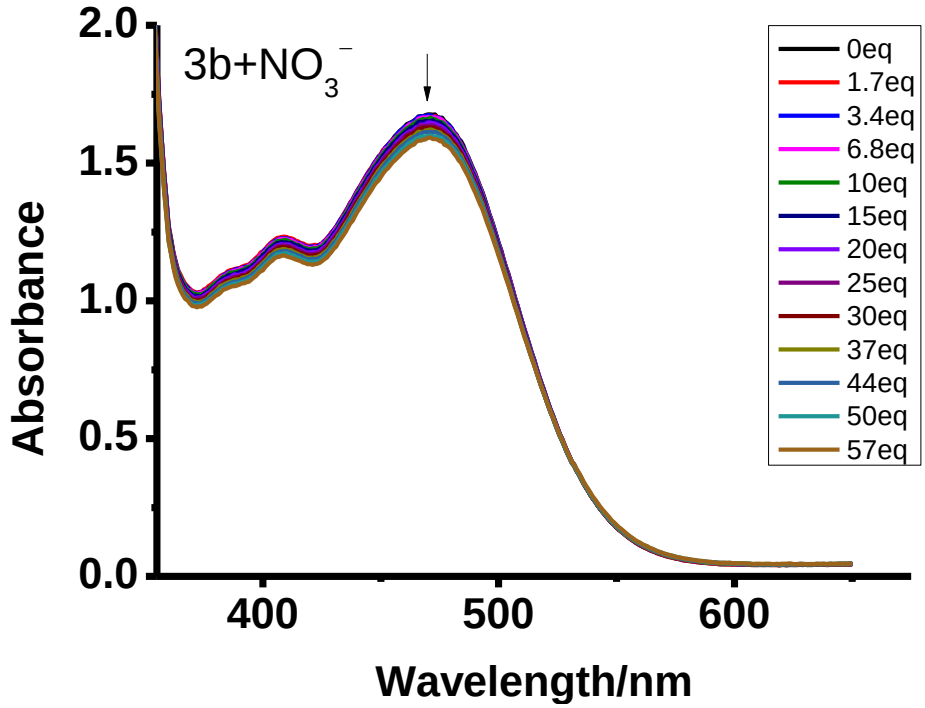

Figure S51. UV–vis spectral changes of **3b** (2.76×10^{-4} mol·dm^{-3}) in DMSO upon addition of NO_3^-.

(a)

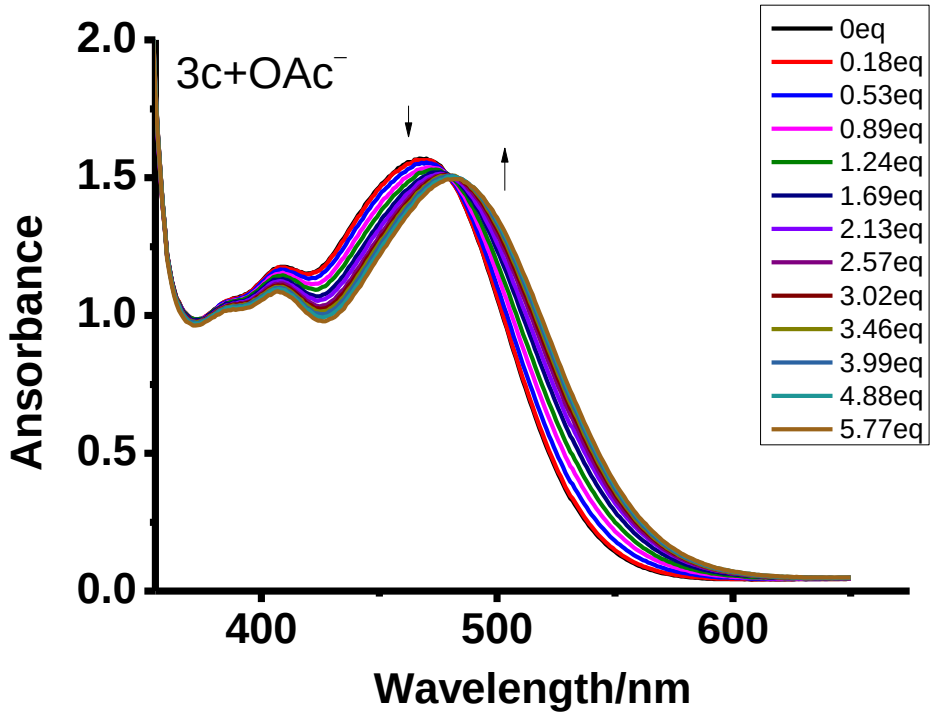

(b)

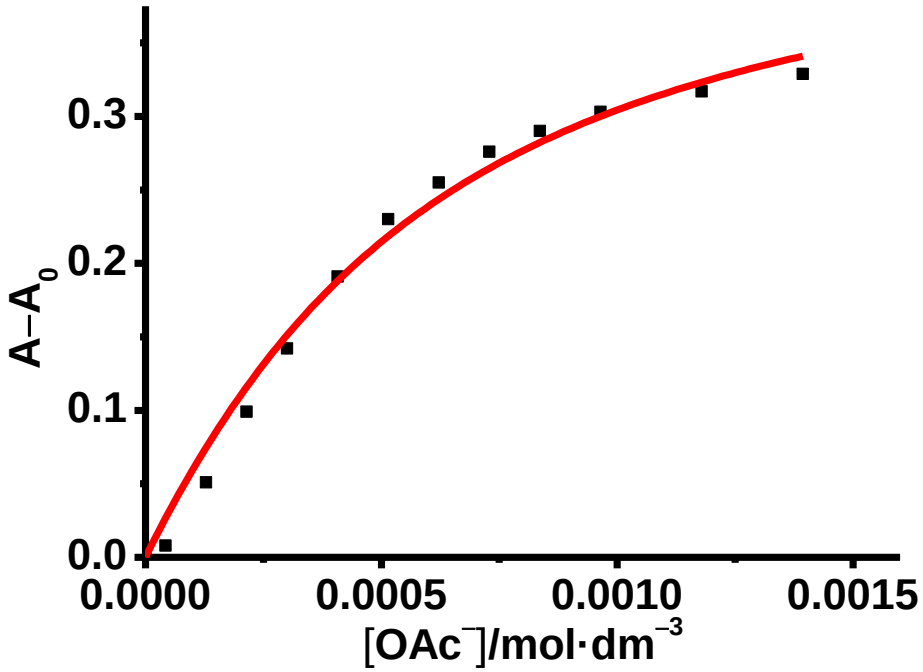

Figure S52. (a) UV–vis spectral changes of **3c** (2.38×10^{-4} mol·dm^{-3}) in DMSO upon addition of OAc^-. (b) A plot of the absorbance change at 540 nm as a function of the concentration of OAc^- and its theoretical fit for the 1:1 binding of complex **3c** with OAc^-.

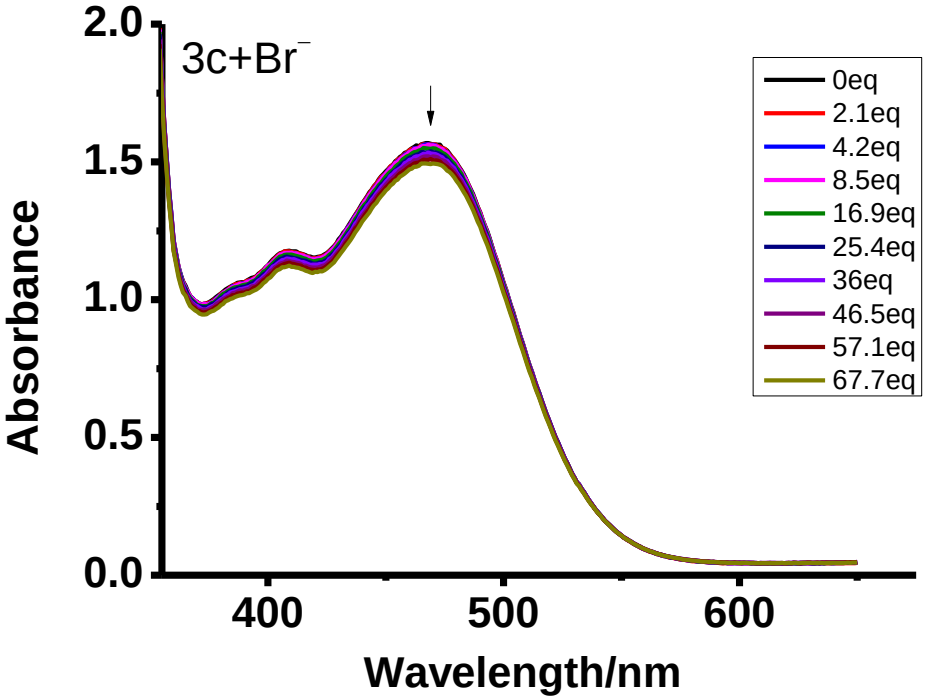

Figure S53. UV–vis spectral changes of **3c** (2.38×10^{-4} mol·dm^{-3}) in DMSO upon addition of Br^-.

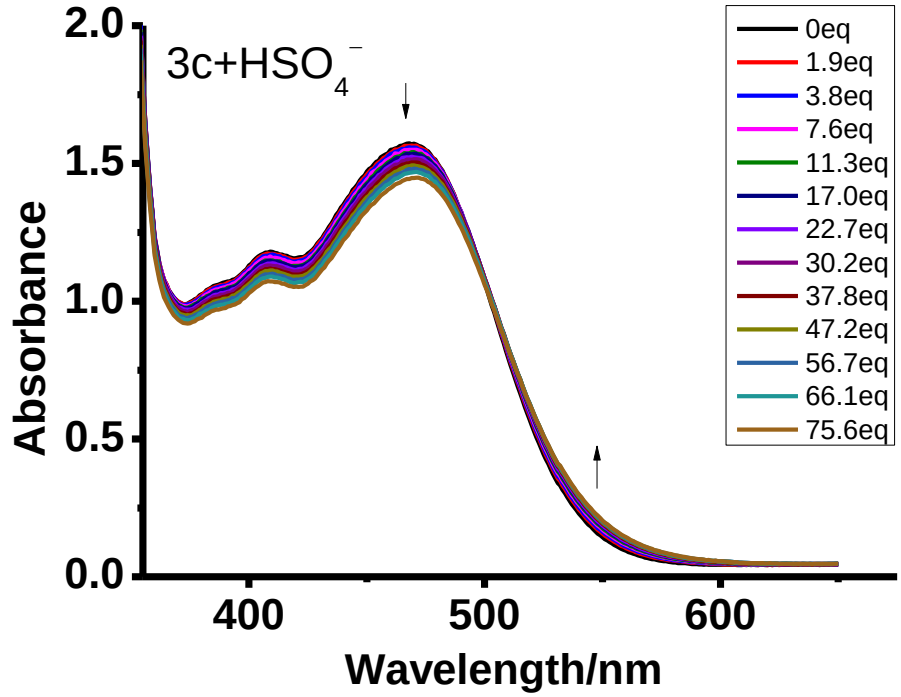

Figure S54. UV–vis spectral changes of **3c** (2.38×10^{-4} mol·dm^{-3}) in DMSO upon addition of HSO_4^-.

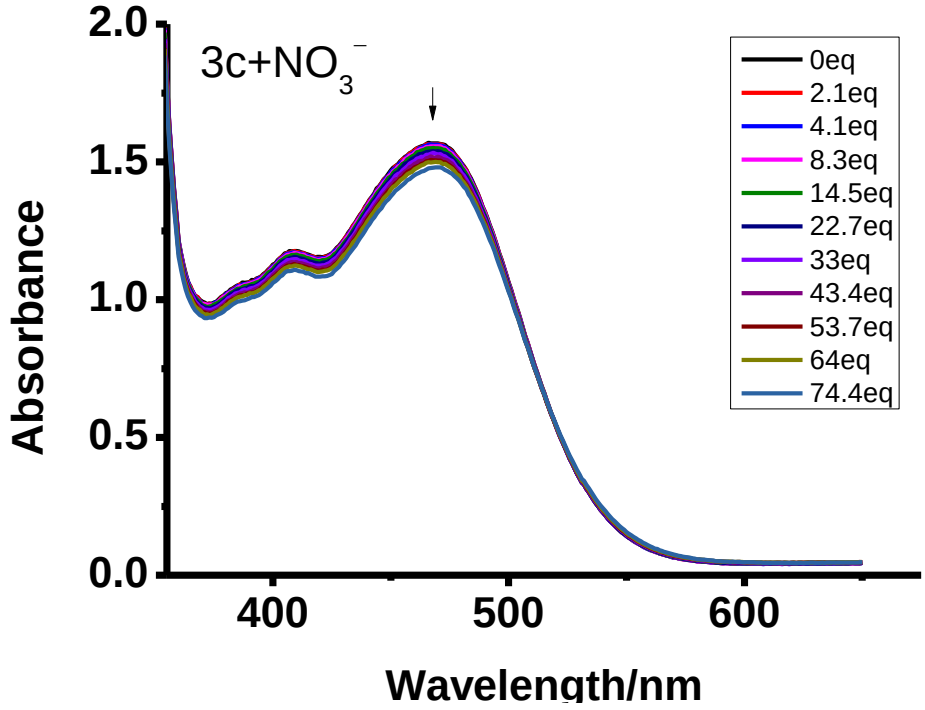

Figure S55. UV–vis spectral changes of **3c** (2.38×10^{-4} mol·dm^{-3}) in DMSO upon addition of NO_3^-.

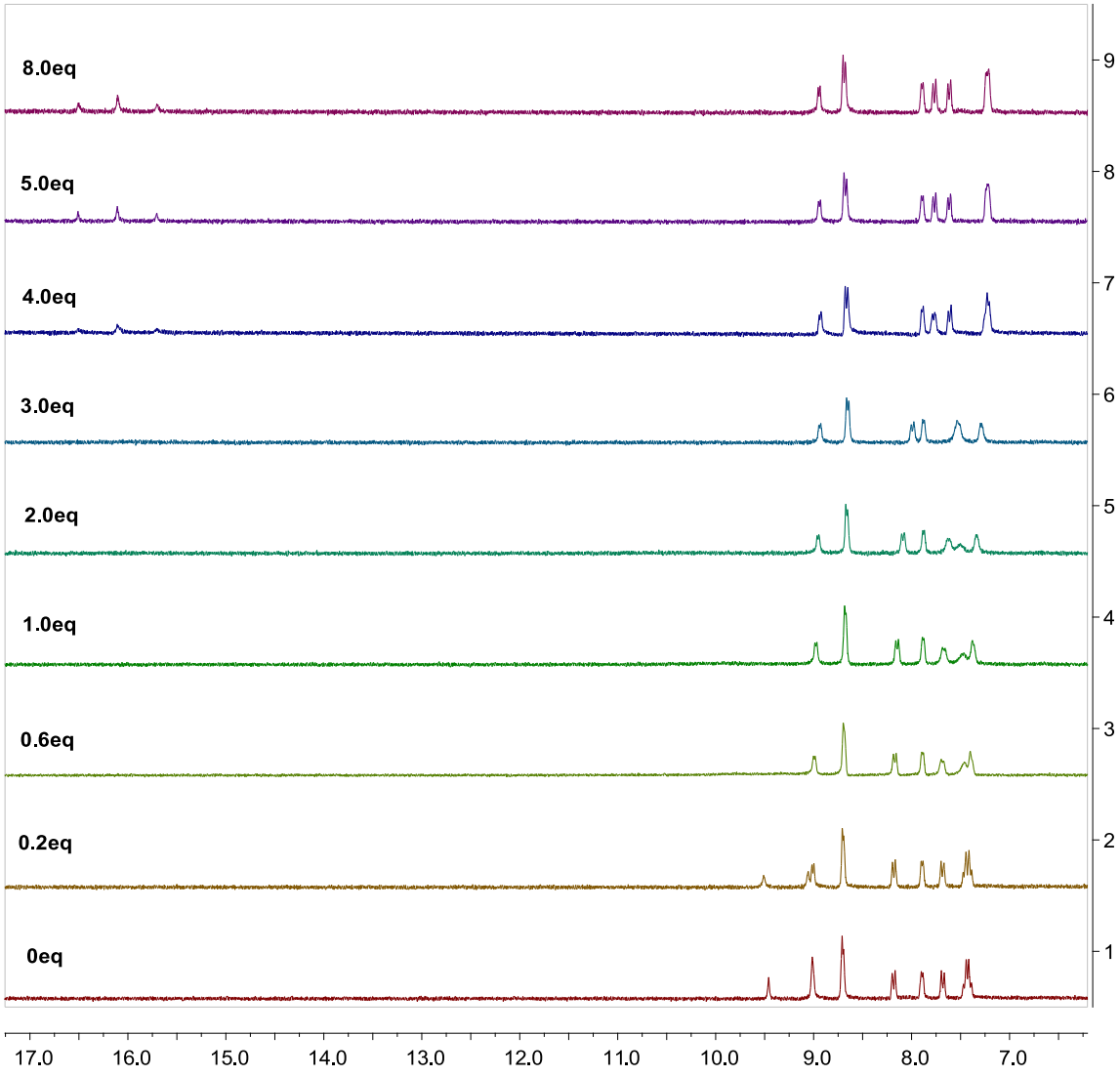

Figure S56. ^{1}H NMR spectral changes of **3d** upon addition of F^{-} in DMSO-d_6 at 6.25–17.25 ppm

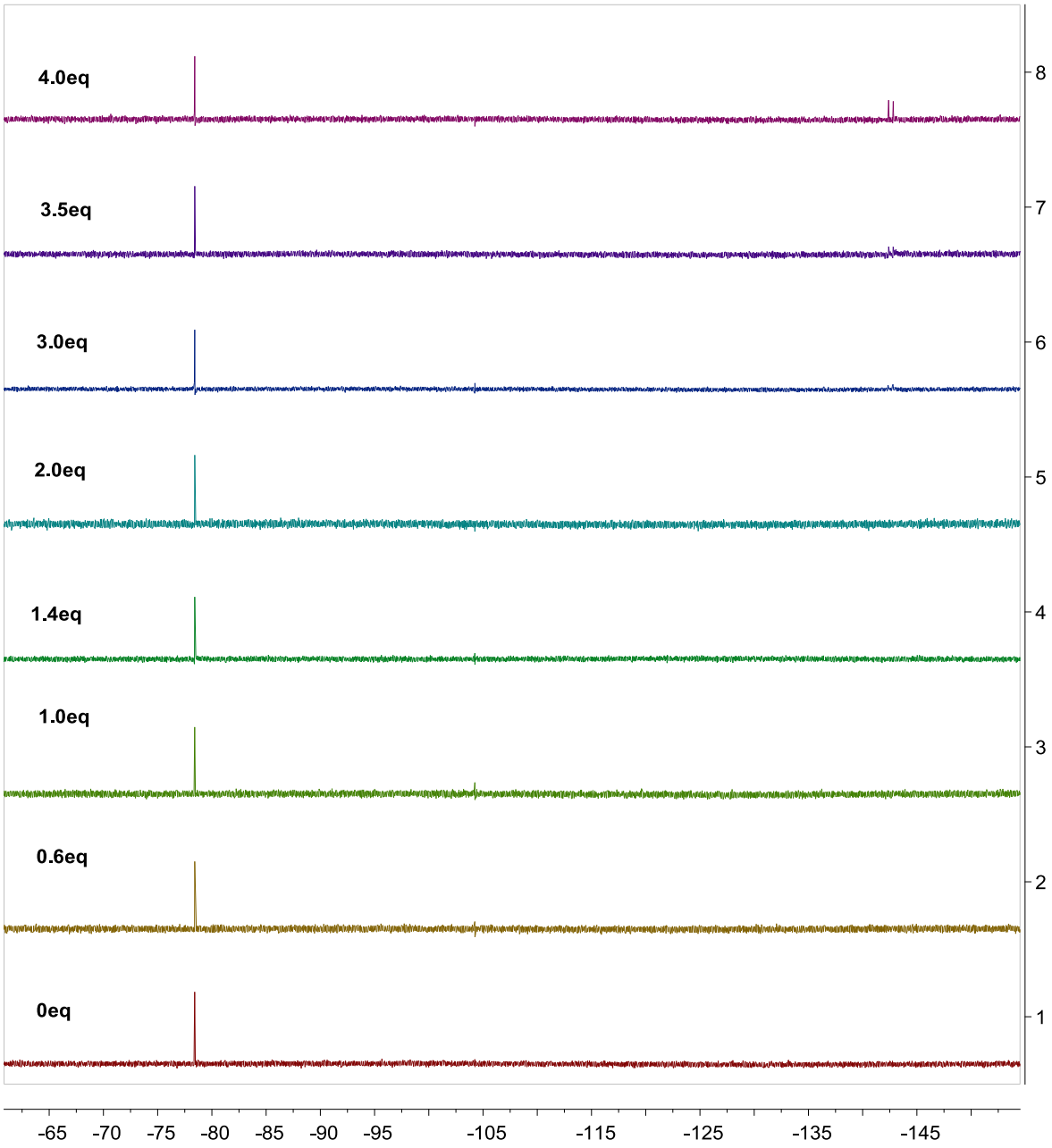

Figure S57. ^{19}F NMR spectral changes of **3d** upon addition of F^- in DMSO-d_6.The singlet at −78.42 ppm comes from the triflate anion.